Journal of Materials Chemistry A

Accepted Manuscript

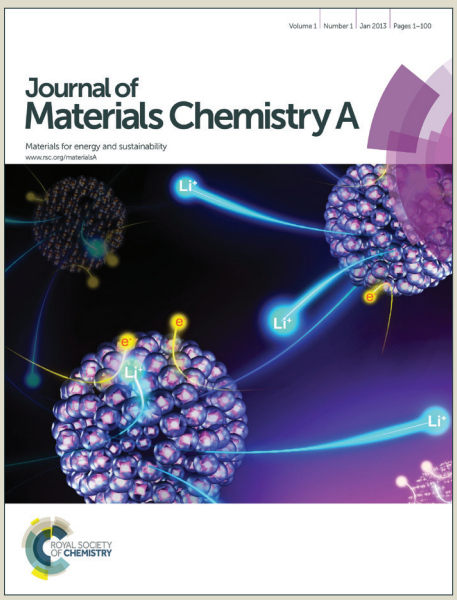

ROYAL SOCIETY OF CHEMISTRY

www.rsc.org/materialsA

Lithium-Sulfur Batteries: from Liquid to Solid Cells

Zhan Lin[1] and Chengdu Liang[2*]

[1]College of Chemical and Biological Engineering, Zhejiang University, Hangzhou, Zhejiang, 310027, China

[2]Center for Nanophase Materials Sciences, Oak Ridge National Laboratory, Oak Ridge, TN 37831, USA

Abstract

Lithium-sulfur (Li-S) batteries supply a theoretical specific energy 5 times higher than that of lithium-ion batteries (2,500 vs. ~500 Wh kg^{-1}). However, the insulating properties and polysulfide shuttle effects of the sulfur cathode and safety concerns of the lithium anode in liquid electrolytes are still key limitations to practical use of traditional Li-S batteries. In this review, we start with a brief discussion on fundamentals of Li-S batteries and key challenges associated with conventional liquid cells. We then introduce the most recent progress in liquid systems, including sulfur positive electrodes, lithium negative electrodes, and electrolytes and binders. We discuss the significance of investigating electrode reaction mechanisms in liquid cells using in-situ techniques to monitor the compositional and morphological changes. We also discuss the importance of this game-changing shift, moving from traditional liquid cells to recently developed solid cells, with positive advances in both solid electrolytes and electrode materials. Finally, the opportunities and perspectives for future research on Li-S batteries are presented.

1. Introduction

Great concerns over the depletion of fossil fuels and the greenhouse effect caused by CO_2 emissions have aroused intense interest in harvesting and delivering more clean energy worldwide, such as wind and solar energies.[1] Critical to the efficient usage of clean energies, electrical energy storage (EES) systems are regarded as an essential element for both stationary power stations and mobile equipment.[2, 3] Among EES systems, rechargeable lithium-ion (Li-ion) batteries have been used widely in portable electronic devices, power tools, and hybrid electric vehicles (HEVs). The crucial shift from current HEVs to all-electrified vehicles (EVs) requires electrical energy storage with a dramatic improvement in specific energy density and power density. However, current Li-ion batteries are not suitable for such requirements because they lack the energy to operate EVs for sufficient range on a single charge.[4-7] Therefore, the transition from the intercalation chemistry in traditional Li-ion batteries to innovative conversion chemistry is needed urgently to overcome challenges of rechargeable lithium batteries.

By replacing the heavy intercalation cathode (such as $LiCoO_2$ or $LiFePO_4$) in traditional Li-ion batteries with a light sulfur cathode, we have lithium-sulfur (Li-S) conversion chemistry in battery cells (i.e., Li-S batteries) with higher specific energy.[8] Since the first introduction in the 1960s,[9] Li-S batteries have been considered a most promising candidate for next-generation energy storage systems

*Corresponding author. E-mail address: liangcn@ornl.gov.

for EVs and large-scale grids because they can supply a theoretical specific energy 5 times greater than that of Li-ion batteries (2,500 vs. 500 Wh kg^{-1}). Moreover, the elemental S is inexpensive, nontoxic, and abundant in nature. Despite these considerable advantages, a great number of scientific and technical challenges are yet to be overcome; numerous R&D programs are invested in developing advanced Li-S cells with excellent longevity as well as high energy and power densities.

Impressive breakthroughs in designing novel electrodes for advanced Li-S batteries have been made, and several good review articles have been published.[10-16] However, most of the review articles focus on the sulfur cathode in traditional liquid cells; research on the lithium anode is largely left unpublished. The possible trend shifting from traditional liquid cells to all-solid cells is also overlooked. In this review, we start with a brief discussion on the fundamentals of Li-S batteries and key challenges associated with the scientific/technical developments of Li-S cells. We introduce the most recent progresses in Li-S battery technology in the liquid system, including sulfur positive electrodes, lithium negative electrodes, electrolytes and binders, and the interlayer design. This review presents effective strategies for longevity of Li-S cells with enhanced energy and power densities and also highlights important breakthroughs in terms of cycle life, stability, and practical electrode loading. We also discuss the significance of investigation of electrode reaction mechanisms in conventional liquid cells using in-situ techniques to monitor the compositional and morphological changes in real time. Then, moving from traditional liquid cells to recently developed solid cells, we discuss this possible game-changing shift with positive advances in both solid electrolytes and electrode materials and discuss the importance of solid design for the practical applications of Li-S batteries. Finally, the opportunities and perspectives for future research on Li-S batteries are presented.

2. Fundamentals of Li-S batteries

In a typical Li-S battery cell, sulfur (S or S_8) and lithium (Li) are used as the positive and negative electrodes, respectively, with liquid electrolyte as both charge transfer medium and ionic conductor within the sulfur-containing cathode.[17-19] Fig. 1 shows a schematic configuration of a typical Li-S cell, which is based on the following conversion reaction:

$$16\ Li + S_8 \leftrightarrow 8\ Li_2S \quad E^o = 2.20\ V\ vs.\ Li/Li^+ \qquad (1)$$

Assuming complete conversion, the sulfur cathode has a theoretical specific capacity of 1,675 mAh g^{-1}; and the whole Li-S cell demonstrates a theoretical energy of 2,500 Wh kg^{-1} or 2,800 Wh L^{-1}.

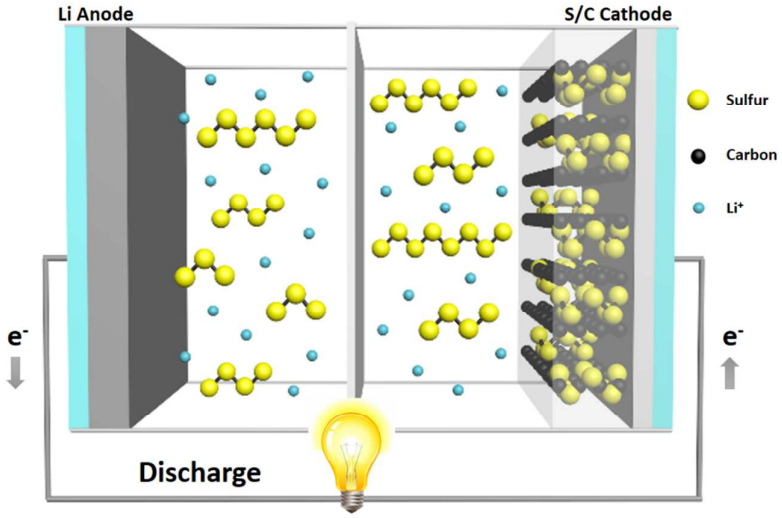

Fig. 1. Schematic configuration of a typical Li-S cell, including the sulfur cathode, the lithium anode, and the liquid electrolyte.

Fig. 2 presents a typical charge-discharge profile in a Li-S cell.[20, 21] During the discharge procedure, two voltage plateaus at 2.4 and 2.0 V, which correspond to the reduction of long chain lithium polysulfides (Li_2S_x, $4 \leq x$) and short chain lithium polysulfides (Li_2S_x, $x \leq 4$), are observed. During the corresponding charging cycle, two plateaus at 2.2 and 2.5 V are observed. Based on the phase transition mechanism, the discharge procedure goes through two stages.[22, 23]

I: Reaction of elemental sulfur with Li forms long chain lithium polysulfides (Li_2S_x, $4 \leq x$), which dissolve in the liquid electrolyte.

$$S_8 + 2\,Li^+ + 2e^- \rightarrow Li_2S_8 \qquad (2)$$
$$3Li_2S_8 + 2\,Li^+ + 2e^- \rightarrow 4\,Li_2S_6 \qquad (3)$$
$$Li_2S_8 + 2\,Li^+ + 2e^- \rightarrow 2\,Li_2S_4 \qquad (4)$$

II: Further reaction between dissolved Li_2S_4 and lithium produces insoluble Li_2S_2 and Li_2S.

$$Li_2S_4 + 2\,Li^+ + 2e^- \rightarrow 2\,Li_2S_2 \qquad (5)$$
$$Li_2S_2 + 2\,Li^+ + 2e^- \rightarrow 2\,Li_2S \qquad (6)$$

During discharge, the reaction in Eq. 4 is affected by both the solubility and the chemical equilibriums of polysulfides in different electrolytes; the final discharge products are primarily a mixture of Li_2S_2 and Li_2S instead of pure Li_2S because of the sluggish kinetics of electrochemical reduction of Li_2S_2 to Li_2S.[16, 24]

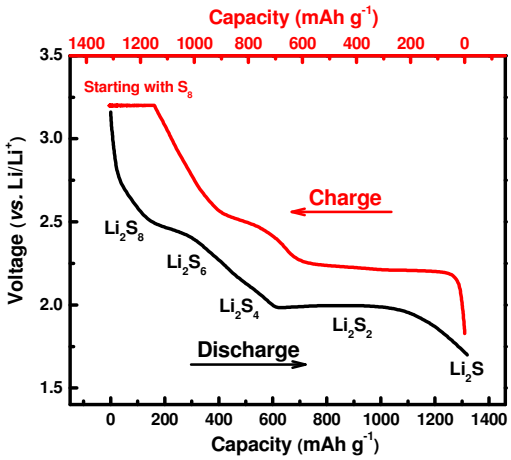

Fig. 2. A typical charge-discharge profile in a traditional liquid Li-S cell.

3. Key challenges of Li-S performance

There are key challenges associated with the performance of Li-S cells.[10, 13, 25] Perhaps the greatest challenge is overcoming the poor electronic and ionic conductivities of S and sulfur discharge products (i.e., polysulfides). A conventional S cathode has low utilization and poor rate capability because of the insulating nature of S (e.g., the electronic conductivity of S is 5×10^{-30} S cm^{-1} at 25 °C). To improve the utilization of active material, carbon materials and/or conducting polymers are used to improve the electronic conductivity of the sulfur cathode. However, the ionic conductivity cannot be improved by such additions. To solve this problem, liquid electrolytes with high solubility of lithium polysulfides are used in conventional Li-S batteries. The utilization of S varies with the solubility of these sulfur species in different liquid electrolytes; i.e., high solubility in the electrolyte accounts for better utilization of the S material. However, a high solubility of sulfur species in liquid electrolytes leads to another prominent challenge for Li-S batteries; i.e., the polysulfide shuttle, which is the transport of sulfur species back and forth between the positive and negative electrodes. The migrated sulfur species chemically react with the lithium anode and cause a "chemical short" in the cell. The "chemical short" leads to the loss of active materials, corrosion of lithium anode (e.g., the insoluble Li_2S accumulates on the Li anode), and low coulombic efficiency. The mobile sulfur species cause the redistribution of sulfur in the cell and impose the third key challenge for Li-S batteries: poor cycle life. The poor cycle life directly relates to the volume change, which accompanies microstructural variations in the electrodes. The mobile sulfur species do not redeposit in their original positions in consecutive cycles. Consequently, the microstructure of the sulfur cathode progressively changes with cycling. The above challenges contribute to the fast aging of electrodes and a quick fading of the practical specific capacity of Li-S batteries.

Self-discharge also is an important challenge for limitation of possible commercialization. There were a few studies for the self-discharge behavior of Li-S cells, including the electrolyte systems of mixed 1,2-dimethoxyethane (DME) and 1,3-dioxolane (DOL), poly(vinylidenedifluoride) and hexafluoropropylene (PVdF-co-HFP), and tetra ethylene glycol dimethylether (TEGDME).[22, 26, 27] Fig. 3 shows the first discharge profiles of Li-S cells using TEGDME as a liquid electrolyte with different storage times at 25 °C. Though the discharge curve has two potential plateaus, the first discharge

capacity continuously decreases with an increase in storage time. Sulfur species dissolve in liquid electrolyte during resting, resulting in self discharge and capacity fading. The level of self-discharge behavior is determined by the shuttle equation (Eq.7):

$$\mathrm{dlnQ/dt} = -k_{\mathrm{S}}, \quad (7)$$

where Q is the plateau capacity, t is the resting time, and k_S is the shuttle constant. In the equation, the self-discharge behavior closely correlates with the shuttle constant, which means that both the shuttle effect and self-discharge effect result from dissolution of active sulfur species in the liquid Li-S cell.

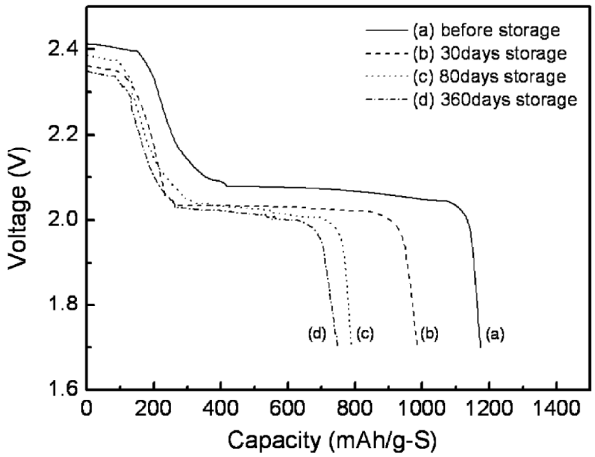

Fig. 3. First discharge profiles of Li-S cells using TEGDME with storage time at 25°C: (a) initial, (b) 30 days, (c) 80 days, and (d) 360 days.[27] Reprinted with permission; © 2006 Elsevier.

Novel designs of electrode materials and cell configurations are needed to conquer the above challenges and improve the cycling performance by inhibiting the dissolution of sulfur species and eliminating the shuttle effect.[28-31] In the following sections, we review and discuss most advances in exploring positive electrodes, negative electrodes, electrolytes/binders, and interlayers in traditional liquid cells, as well as solid electrolytes and electrode materials in recently developed solid cells for the longevity of high specific energy Li-S batteries.

4. Traditional liquid cells

In traditional Li-S cells, carbon materials or conducting polymers with liquid electrolytes are used to conquer the challenges associated with sulfur cathodes.[32, 33] However, use of liquid electrolytes always leads to the polysulfide shuttle.[34] In this section, we review and discuss the most recent advances in electrochemical performance of traditional Li-S cells from the different cell components: sulfur positive cathodes, lithium negative anodes, electrolytes and binders, and interlayers. We then discuss the significance in investigating electrode reaction mechanisms using in-situ techniques to monitor the compositional and morphological changes in the electrodes in real time.

4.1. Sulfur positive electrodes

Because the electronic conductivity of S is relatively low (5×10^{-30} S cm^{-1}), conducting materials such as carbons or conducting polymers are necessary to improve its conductivity for good utilization and excellent cycling. A conductive network is formed for enhancement of the cathode conductivity, which offers high specific surface area for electron transport between the sulfur and conducting host. The high surface area and/or porous structure also benefit the sulfur adoption and prevent polysulfides from dissolving into electrolytes. Based on compositions and structures, herein we divide traditional sulfur materials into three categories: (1) carbon sulfur composites, (2) polymer sulfur composites, and (3) lithiated sulfur materials. In the following subsection, we discuss technical approaches with specific examples to highlight important progress toward high-performance Li-S cells, such as improved energy and power density with good long-term cycling.

4.1.1. Carbon sulfur composites

Shortly after the discovery by Nazar[35] of highly ordered composites of sulfur and mesoporous carbon (CMK-3) as sulfur cathode materials, various porous carbon-sulfur composites were investigated, and more improvements in cycling were reported. Based on structures, here we discuss carbon materials in three categories: (1) porous carbons, (2) graphene or graphene oxides, and (3) hybrid carbons. Many research articles have been published on various carbons for high-performance Li-S batteries.[36-61] We just choose some representatives in each category to highlight the improvements in cycling performance.

4.1.1.1. Porous carbons

Among various carbon materials such as one-dimensional nanotubes/nanowires, two-dimensional graphene, and three-dimensional hierarchically structured carbons,[62, 63] porous carbons with high surface are received considerable attention for Li-S battery cathodes. The porous structure and high electrical conductivity are essential criteria for simultaneously accommodating active sulfur species and enhancing cathode conductivity. Based on pore size and morphology, the porous carbons are classified into three categories: (1) the micropore ($D\leq2$ nm), (2) the mesopore (2 nm$\leq D\leq$50 nm), and (3) the macropore ($D\leq50$ nm). Each type of porous carbons possesses unique properties and morphological advantages.

The microporous carbon. The sulfur loss can be diminished effectively by accommodating and immobilizing the active material in the microporous carbon. Metastable small sulfur molecules such as S_{2-4} were synthesized by Xin et al.[64] in the confined space of a conductive microporous carbon matrix. The microporous carbon matrix consisted of a coaxial structure with a carbon nanotube core and ~100 nm microporous carbon sheath (CNT@MPC). Based on the cumulative pore volume for the micropores (<0.6 nm), the calculated sulfur loading in the micropores is ~49 wt%. When used with a carbonate-based electrolyte, the S/(CNT@MPC) composites showed one plateau that was attributed to the electrochemical reversibility of S_{2-4} (Fig. 4a). The initial discharge capacity of 1,670 mAh g^{-1} (normalized to S) was obtained at C/10, which is much higher than that of S/carbon black. The capacity was still much higher than 1,000 mAh g^{-1} after 200 cycles; the coulombic efficiency remained ~100% (Fig. 4b). The S/(CNT@MPC) composite cathode prevents the unfavorable transition between S_8 and

S_4^{2-}, which in turn prevents the polysulfide shuttle and subsequently improves capacity retention. These Li-S cells exhibit unprecedented electrochemical behavior with high specific capacity and good cycling stability.

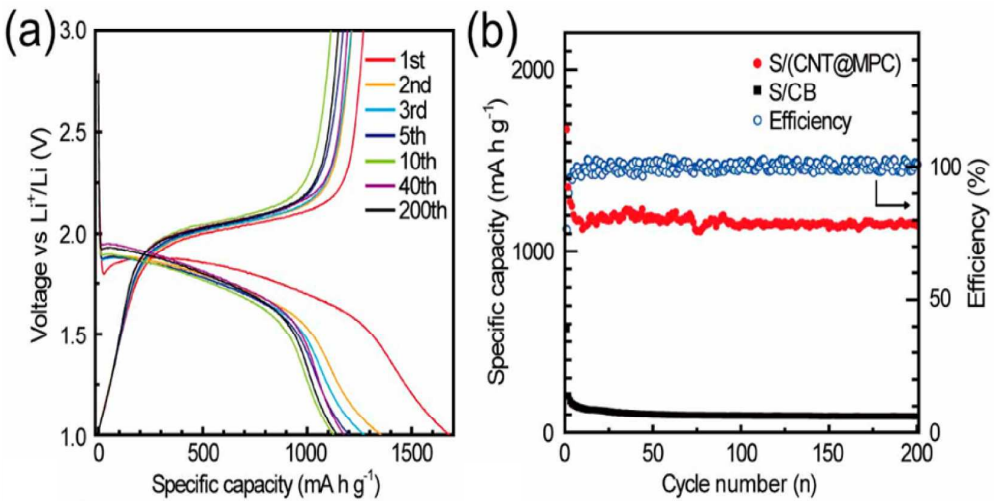

Fig. 4. (a) The charge-discharge profiles of S/(CNT@MPC) at C/10. (b) Cycling performance and coulombic efficiency of S/(CNT@MPC) and S/CB at C/10.[64] Reprinted with permission; © 2012 American Chemical Society.

The mesoporous carbon. The mesoporous carbon in Fig. 5 was identified as an ordered encapsulation substrate for sulfur loading.[65, 66] The spherical mesoporous carbon nanoparticles were obtained in a two-step casting process.[67] An opal structure of poly(methyl methacrylate) (PMMA) spheres was cast with a silica precursor solution to form a silica inverse opal (Fig. 5a). The inverse opal was used as a template for a tri-precursor solution containing resol as the carbon precursor, tetraethylorthosilicate as the silica precursor (Fig. 5b), and the block copolymer Pluronic F127 as a structure-directing agent. Etching of the silica template and the silica in the carbon/silica nanocomposite through carbonization formed ordered mesoporous carbon (OMC) with hierarchical porosity (Fig. 5c). When OMC was used as a cathode material for Li-S batteries, an excellent cycling was demonstrated when the sulfur loading is up to 70 wt%. S-BMC/S-70-W shows the highest reversible discharge capacity of 1,070 mAh g^{-1} (Fig. 5d). After 100 cycles, this cell still maintains a capacity of 860 mAh g^{-1} at a high current density of 1C. The mesopores enhance sulfur encapsulation and improve lithium ion and electrolyte transport as well as raise tolerance toward high sulfur loading.

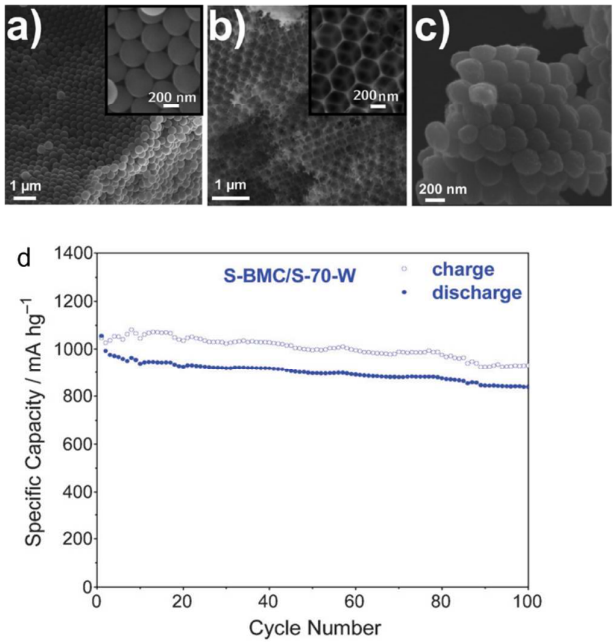

Fig. 5. Scanning Electron Microscope (SEM) images of (a) ordered PMMA spheres with an inset at higher magnification, (b) silica inverse opal structure with an inset at higher magnification, and (c) OMC spheres ordered in opal structure. (d) Discharge and charge capacity of S-BMC/S-70-W.[67] Reprinted with permission; © 2012 WILEY-VCH Verlag GmbH & Co. KGaA, Weinheim.

The macroporous carbon. The macroporous carbon is usually derived from an interwoven network of carbon nanotubes (CNTs) or carbon nanofibers. Zhang et al. synthesized porous nitrogen-doped CNTs with the inner diameter of 55 nm.[68] This carbon has a high specific surface area of 1,765 m^2 g^{-1} and a large pore volume of 1.28 cm^3 g^{-1}, and it demonstrated an initial discharge capacity of 1,341 $mAhg^{-1}$ at 1C when used as cathode for Li-S cells. Even after 50 cycles, the high reversible capacity was retained at 933 mAh g^{-1}. The macropores ensure excellent electrolyte immersion and suppress polysulfide migration because of their high electrolyte absorbability. Using anodic aluminum oxide membranes as templates for disordered carbon nanotubes (DCNTs), sulfur-DCNT (SDCNT) composites were reported by Wang et al. as cathode materials for Li-S cells.[69] The graphitic clusters and amorphous carbon structures of DCNTs were easily accessible by S vapor, and they serve as both the host for sulfur and the barrier for liquid electrolyte. A solution of sulfur in carbon disulfide was dripped on top of DCNTs and then dried to form SDCNT composites. The sulfur impregnation was carried out by heating the SDCNTs in vacuum at 160 °C (SDCNT-160), 300 °C (SDCNT-300), and 500 °C (SDCNT-500). SDCNT-160 demonstrated typical cyclic voltammetry (CV) behavior as a traditional sulfur cathode: three cathodic peaks indicated the reduction of S_8 to S_6^{2-}, S_4^{2-}, and S_2^{2-}(or S^{2-}). In comparison, only two oxidation peaks were identified in SDCNT-300 and SDCNT-500, and a new broad peak, which was lower than the reaction potential of S_4^{2-} to S_2^{2-} at 1.95 V, was found at 1.8 V. The new broad peak at 1.8 V in both SDCNT-300and SDCNT-500 could be attributed to conversion of S_2^{2-} to S^{2-} and could be an indication of strong bonding between sulfur and carbon. The SDCNT-500 cathode had the best cycling stability, i.e., 73% retention after 100 cycles and

coulombic efficiency of 96%. The improvement indicates the profound effect of the heat treatment. Sulfur was incorporated in voids/graphite layers in the partially graphitized DCNTs structure at higher temperature (i.e., 500 °C), which prevented the direct contact of S with the liquid electrolyte. The possible sulfur-carbon bonding and the existence of smaller sulfur structures (e.g., S_6 and S_2) induced by higher-temperature heat treatment could enhance the longevity of Li-S batteries.

4.1.1.2. Graphene or graphene oxides

As a two-dimensional carbon representative, graphene was used as a conducting material and polysulfide reservoir for sulfur species because it has the merits of both high electronic conductivity and large surface area.[70] Zhou et al. prepared a graphene-sulfur-graphene sandwich structure with pure sulfur between two graphene membranes (Fig.6).[71] One graphene membrane as a current collector (GCC) was coated with sulfur as the active material, while the other graphene membrane was coated on a commercial separator (G-separator). The sulfur loading is up to 70% in the electrode. In this sandwich-structured cathode, two graphene layers not only provided high electric conductivity and buffered the large volume change of sulfur active material but also acted as polysulfide reservoirs during cycling. As a result, an initial high discharge capacity of 1,345 mAh g^{-1} and a capacity greater than 1,000 mAh g^{-1} over the 50 cycles were reported. Moreover, GCC had a much lower density than an Al-foil current collector, and they could improve the specific energy density of a Li-S cell. This research activity demonstrates the importance of introducing a simple but effective way for high-performance Li-S batteries.

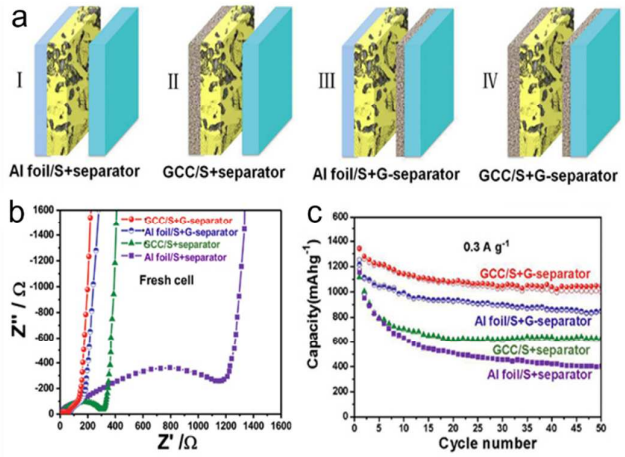

Fig. 6. (a) Schematic of electrode configurations of: (I) an Al foil, sulfur cathode, and commercial separator (Al foil/S+separator); (II) a GCC, sulfur cathode, and commercial separator (GCC/S+separator); (III) an Al foil, sulfur cathode, and G-separator (Al foil/S+G-separator); and (IV) a GCC, sulfur cathode, and G-separator. (b) Nyquist plots of the electrode in different configurations. (c) Cycling performance with different configurations at a current density of 300 mA g^{-1} for 50 cycles.[71] Reprinted with permission; © 2013 WILEY-VCH Verlag GmbH & Co. KGaA, Weinheim.

Graphene also has the ability to marry sulfur with various surface functionalization methods, such as the oxidation on its surface to introduce oxygen functional groups; i.e., graphene oxide (GO).

GO/sulfur particles were wrapped in GO with arbitrary sizes, geometries, and compositions by using a facile method of coating. This method does not involve any chemical reaction between GO and sulfur, but rather requires a driving force because of the tendency of lowering the surface energy of GO.[72] Ji et al. used a low-cost, environmentally benign strategy to chemically immobilize S on GO by preparing GO-S nanocomposites for Li-S cells.[73] Sulfur nanoparticles were deposited onto GO sheets by chemical reaction in a micro-emulsion system, which reliably provided intimate contact between sulfur and carbon. After heat treatment, sulfur melts and diffuses into the pores of GO because of strong adsorption effects from both high surface area and functional groups on the GO. When applied as a cathode material for Li-S cells, the GO-S nanocomposites showed excellent electrochemical performance; e.g., the capacity of >1,000 mAh g^{-1} was obtained after 55 cycles (Fig. 7a). This improvement was attributed to the unique structure of the GO with various functional groups, which strongly anchor sulfur atoms and effectively prevent lithium polysulfides from dissolving into electrolytes. This was confirmed by ab initio calculations and X-ray absorption spectroscopy (XAS) measurements shown in Figs. 7b-7c. Hydroxyl and epoxy groups enhance the binding between S and C atoms because of the induced ripples on the flat graphene surface by functional groups.

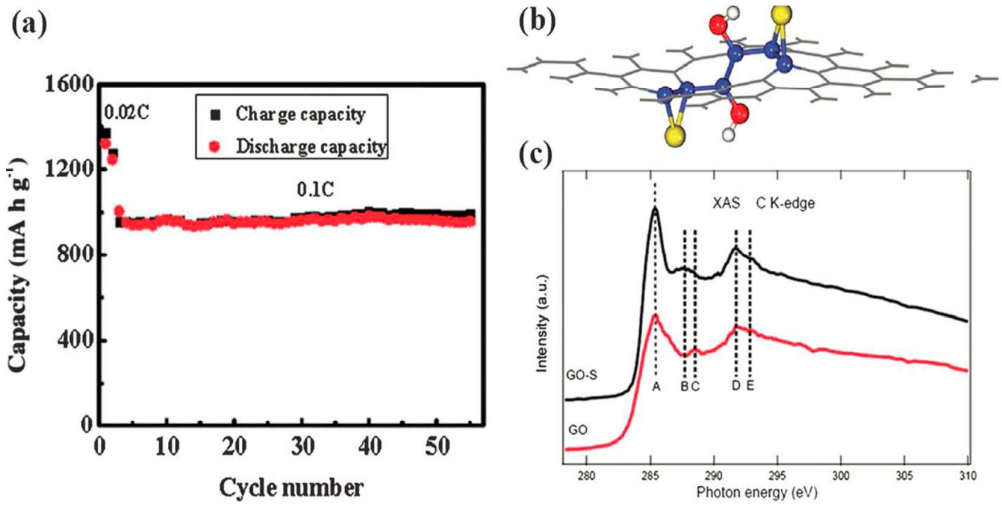

Fig. 7. (a) Cycling performance of the GO-S cathode. (b) Representative simulation of GO-immobilized sulfur. Yellow, red, and white balls represent S, O, and H atoms, while others are C atoms. (c) C K-edge XAS spectra of GO and GO-S composites after heat-treatment.[73] Reprinted with permission; © 2011 American Chemical Society.

Though graphene or graphene oxide showed effectiveness in enhanced cyclability of Li-S cells by improving the conductivity of sulfur cathode and confining the polysulfides at the cathode, the rate capabilities of these cathode materials are far from ideal.[45, 74] For example, the GO-S composite electrodes mentioned above exhibited an acceptable reversible capacity of 370 mAh g^{-1} at 2C, but their rate capability was insufficient for use in high-power applications such as electric vehicles.[73] To achieve high power density of Li-S cells, a suitable carbon architecture and nanostructure need to be synthesized to enhance fast charge transfer across interfaces and rapid transport of Li-ions to active sites for electrode reactions.

4.1.1.3. Hybrid carbons

Porous carbons and graphene reserved the dissolved polysulfides in the cathode and gave the sulfur cathode a new lease on life. However, most of them are in the amorphous state and sp^3-hybridized C-C bonding, and therefore exhibit relatively poor electrical conductance. Hybrid carbon materials that combine highly conductive carbon nanomaterials with porous carbons can achieve better performance of sulfur-carbon electrodes. Peng et al. designed nanoarchitectured graphene/CNT@porous carbon with excellent electrical conductivity and interconnected micro-/mesopore structures.[75] The sp^2graphene/CNT interlinked networks give the composites good electrical conductivity and a robust framework, while the strong confinement induced by micro-/mesopores restrained the shuttle phenomenon for high capacity retention. The composite cathode exhibited an ultrahigh specific capacity of 1,121 mAh g^{-1} at C/2 and an impressive cycling stability of 877 mAh g^{-1} after 150 cycles at 1C. Based on the total mass of packaged devices, gravimetric energy density of the cell is expected to be 400 Wh kg^{-1} at power density of 10,000 W kg^{-1}, matching the level of engine driven systems. Recently, Zhao et al. encapsulated multiwall nanotubes (MWNTs) into hollow porous carbon nanotubes to prepare a tube-in-tube carbon nanostructure cathode (S-TTCN) for Li-S cells (Fig. 8a).[76] The S-TTCN composite cathode exhibited excellent cycling stability and a high discharge capacity of 918 mAh g^{-1} after 50 cycles at a current density of 500 mA g^{-1} (Fig. 8b). The discharge/charge columbic efficiency remained at ~98% during cycling. Based on the overall mass of S-TTCN, this composite delivered a high capacity of 652 mAh g^{-1} after 50 cycles. The MWNTs improve the electronic conductivity and capacity, while the porous carbon layers effectively inhibit the polysulfide dissolution and capacity retention during cycling.

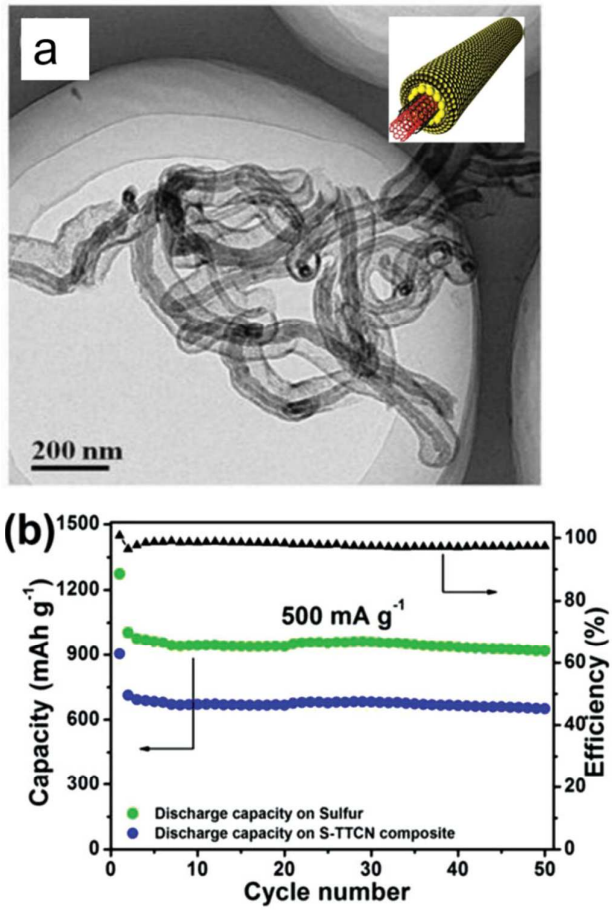

Fig. 8. (a) Schematic illustration and high-resolution Transmission Electron Microscope images of S-TTCN composite. (b) Cycling performance of S-TTCN at 500 mA g^{-1}.[76] Reprinted with permission; © 2014 WILEY-VCH Verlag GmbH & Co. KGaA, Weinheim.

4.1.1.4. Other carbon materials

In addition to the above three categories of carbon materials, other novel structured carbons, such as 3D structured carbon,[52, 77] carbon with hollow structures,[78] hyperbranched carbon nanorod architectures,[79] were also designed for high performance Li-S batteries. Wang et al. reported 3D composite carbon-sulfur materials, consisting of porous pyrolyzed polyacrylonitrile-sulfur@graphene nanosheet (pPAN-S@GNS).[52] The pPAN-S primary nanoparticles are wrapped homogeneously and loosely within a three-dimensional network of graphene nanosheets (GNS). The sulfur loading in the composite is about 50%. The hierarchical pPAN-S@GNS composite shows an initial high reversible capacity of 1,449 mAh g^{-1} and capacity retention of 88.8% after 300 cycles at C/5. A remarkable capacity of near 700 mAh g^{-1} is obtained at a high discharge rate of 10C. The spherical secondary GNS structure creates an electronically conductive 3D framework and reinforces structural stability for superior-performance Li-S cells. Xiao et al. developed a double layered core-shell structure of polymer-coated carbon-sulfur composites, which impregnate sulfur into hollow carbon spheres under

heat treatment, followed by a coating polymerization to give a double-layered core.[80] The sulfur not only penetrated through the porous carbon shell but also aggregated along the inner wall of the carbon shell (Fig. 9). The electrode was made with a loading of ~1.5 mg cm^{-2} sulfur. A stable capacity of 900 mAh g^{-1} at C/5 after 150 cycles and 630 mAh g^{-1} at 0.6 C after 600 cycles are obtained. This is attributed to the desirable confinement of sulfur through the unique double-layered core-shell architectures. More recently, the synthesis of 3D hyperbranched hollow carbon nanorod encapsulated sulfur nanocomposites as cathode materials for Li-S batteries was reported by Wang et al.[79] The sulfur nanocomposite cathodes deliver a high specific capacity of 1,378 mAh g^{-1} at C/10 and excellent high rate capacities and cyclability, such as 990 mAh g^{-1} at 1C, 861 mAh g^{-1} at 5C, and 663 mAh g^{-1} at 10C for more than 500 cycles. The unique 3D hyperbranched hollow carbon nanorod architectures effectively prevent dissolution of polysulfides, decrease self-discharge, and confine volume expansion on cycling. High capacity, excellent high-rate performance, and long cycle life render the above three nanostructured carbons promising cathode materials for Li-S batteries.

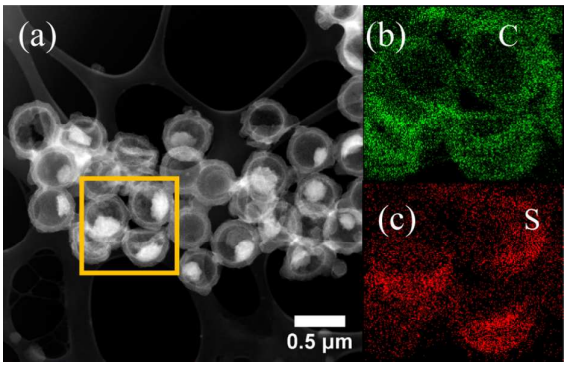

Fig. 9. STEM (a) image of NHC-S composite and elemental mapping of carbon (b) and sulfur (c) of the region shown in the yellow square.[80] Reprinted with permission; © 2014 American Chemical Society.

4.1.2. Polymer sulfur composites

Compared with the high temperature required in the fabrication of carbon materials (e.g., >600 °C), the synthesis of polymer materials is feasible at temperatures below 100 °C. Polymer coating is a viable low temperature approach to trap S and polysulfides in the cathode. The functional groups and unique chain structure of polymers further improve the effectiveness in chemically confining sulfur and polysulfides to the cathode.[81, 82] Polymers with conducting properties are good candidates in fabrication of polymer-sulfur composites because of their high conductivity and good compatibility with S.[83]

Polyaniline. Polyaniline (PANI) is a conductive polymer for making S-PANI composites. PANI works as either a conductive coating layer or matrix after pyrolization. Gao et al. coated sulfur/carbon black (S/C) composites with PANI by an in-situ chemical oxidative polymerization of aniline monomer. These composites have S/C as the core and PANI as the shell, with a thickness of 5-10 nm.[84] The composites with 43.7% sulfur present the optimum electrochemical performance. When the S/C@PANI composite was applied as a cathode, it showed a high initial discharge capacity of 1,405 mAh g^{-1} and a capacity of 596 mAh g^{-1} after 100 cycles. In sharp contrast, the initial discharge capacity of the S/C composite was only 820 mAh g^{-1}, indicating a lower utilization of 49% for active material.

The unique core/shell structure in the S/C@PANI composite was responsible for the improvement of the electrochemical performance. Because of synergistic effects on the high electrical conductivity from both conductive carbon black in the core and the PANI coating on the surface, an excellent discharge capacity of 636 mAh g^{-1} and capacity retention of 60% after 200 cycles was still retained for the S/C@PANI composite at an ultrahigh rate of 10C. Recently, Zhou et al. prepared yolk-shell structure of PANI-coated sulfur for Li-S batteries through a heating vulcanization of a polyaniline-sulfur core-shell structure (Fig. 10a).[85] The sulfur loading in the composites is about 58 wt%. This treatment was much more effective than chemical leaching to prepare uniform yolk-shell structures (Fig. 10b). Compared with its sulfur-polyaniline core-shell counterparts, the yolk-shell nanostructures delivered much improved cyclability owing to presence of internal void space inside the polymer shell to accommodate the volume expansion of sulfur during lithiation. The yolk-shell material exhibited a stable capacity of 765 mAh g^{-1} at C/5 after 200 cycles (Fig. 10c). This result represents important insights and novel methodology to confine sulfur and polysulfides for possibly industrial Li-S batteries.

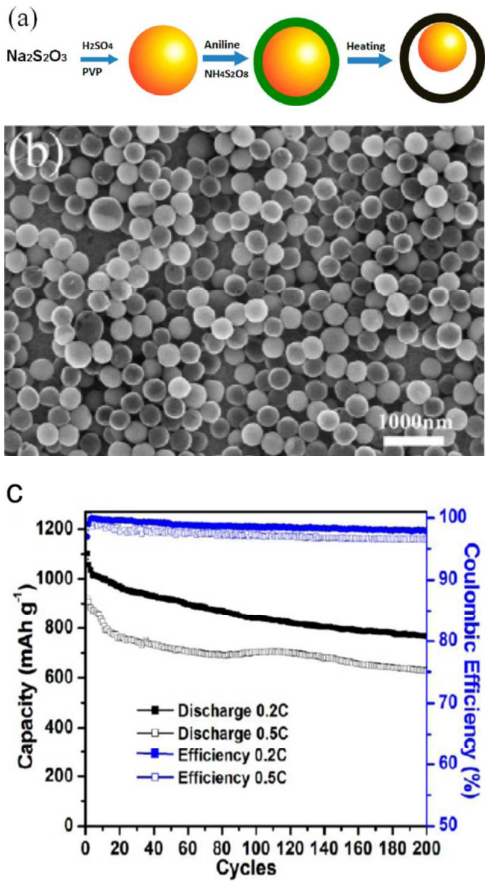

Fig. 10. (a) Schematic of synthesis route for S-PANI composites (the yellow sphere represents sulfur, the dark green shell represents polyaniline, and the black shell represents vulcanized polyaniline). (b) SEM images of the S-PANI core-shell composites. (c) Cycling performance of S-PANI composite cathodes at a rate of C/5 and C/2.[85] Reprinted with permission; © 2013 American Chemical Society.

Polypyrrole. Polypyrrole (PPy) is electrochemically active in a voltage range of 2-4 V vs. Li/Li^+, and therefore, is widely used in various high energy density battery systems. Ma et al. encapsulate sulfur into a thin wall, hollow, spherical structured polypyrrole (T-HSSP) to prepare S@PPy composites (Fig. 11a).[86] The composite with a sulfur content of 58.4 wt% exhibits a reversible capacity of 1,563 mAh g^{-1} and a discharge capacity retention over 89% during 40-200 cycles (Fig. 11b). The excellent rate capability of the composite is demonstrated at 1, 2, and 5C for 300 cycles. The capacity after 300 cycles is about 74.6%, 78.8%, and 83.3% of each corresponding capacity at the 40th cycle at 1, 2, and 5C. The T-HSSP buffers the volume expansion of sulfur and maintains integrity of the sulfur electrode during cycling. The distribution of the sulfur component is maintained even after 100 charge/discharge cycles, indicating the efficiency of the design in inhibiting the shuttle effect of the sulfur electrode.

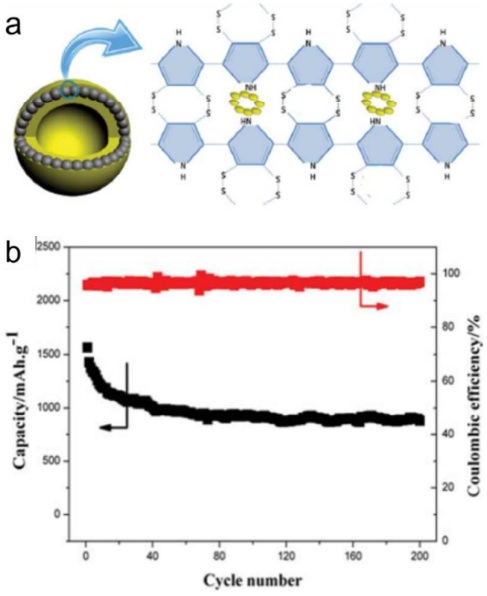

Fig. 11. (a) Schematic of possible structure for S@PPy composite. (b) The discharge capacity and coulombic efficiency of S@PPy-300 cathode at 1C.[86] Reprinted with permission; © 2014 Royal Society of Chemistry.

Other polymers. Except for the above conducting polymers, other polymers[87-95] such as copolymers or polyacrylonitrile (PAN)[96-98] also were used as a coating protective layer for the sulfur cathode. By using the chemical oxidation method with cetyltrimethyl ammonium chloride as a template, Qiu et al. prepared poly(pyrrole-co-aniline) (PPyA) copolymer nanofibers as a conductive matrix for the sulfur cathode.[99] Sulfur was heated with PPyA copolymer nanofibers to prepare the composite materials at 160 °C for 24 h. The copolymer nanofibers have a unique porous structure with high surface area (78 m^2 g^{-1}) for absorbing sulfur and confining polysulfides; the conducting matrix has a good electronic conductivity (58 S cm^{-1}) to compensate for the insulating nature of sulfur. The resulting S/PPyA composites exhibited an initial capacity of 1,285 mAh g^{-1} and good capacity retention of ~70% after 40 cycles. Wang et al. synthesized PAN-S composite cathode for Li-S batteries.[100] By adding 4 wt% graphene in the composite, PAN nanoparticles with less than 100 nm in size, were anchored on the

surface of the grapheme. The resulting composite cathode exhibited a reversible capacity of 1,500 mAh g^{-1} sulfur or 700 mAh g^{-1} composite at the first cycle, corresponding to a sulfur utilization of 90%. More recently, Chen et al. prepared sulfur/polyacrylonitrile (S/PAN) composite by manual mixing of sulfur and PAN followed by heat-treatment at 300 ^{o}C in argon.[96] The sulfur loading in the composites is 48 wt%. The S/PAN cathodes exhibit a stable discharge capacity of 1,050 mAh g^{-1} after 80 cycles at C/5, and good rate performance with up to 770 mAh g^{-1} at 1C. The retained long chains of PAN during synthesis should contribute to the enhanced electronic conductivity of the composite and the subsequent improved cycling performance.

4.1.3. Prelithiated sulfur materials

Issues surrounding the lithium anode also are important when developing new technology for improvements in conductivity and cycle life. There have long been safety concerns associated with the metallic lithium anode because of its high reactivity with liquid electrolytes and tendency for dendrite formation during Li plating.[101] Lithium sulfide (Li_2S) has been used as a pre-lithiated sulfur cathode[102-104] because it has a high theoretical capacity of 1,166 mAh g^{-1} and a much higher melting point than that of sulfur (938 vs. 115 °C). This allows for the use of high temperature heat treatment to protect the sulfur cathode and prevent sulfur species from dissolving in liquid electrolytes. A Li_2S cathode also could act as the lithium source and avoid the direct use of a metallic lithium anode. The possible combination of Li_2S cathode with Si or Sn anode can dramatically enhance safety without compromising energy density of rechargeable Li-S batteries.[105, 106]

Micro-Li_2S. Bulk Li_2S (also micro-Li_2S) has electronic and ionic conductivities as low as 10^{-14} and 10^{-13} S cm^{-1}, respectively; it was always considered as an electrochemically inactive material. Cui et al. reported a Li_2S composite cathode composed of a micro-Li_2S filled mesoporous carbon (CMK-3).[105] The CMK-3 nanorod network provided electronic access to Li_2S, solving the problem of the slow kinetics of Li_2S-based cathodes. When the Li_2S/CMK-3 composite cathode was combined with a silicon nanowire anode, this new battery chemistry demonstrated a theoretical specific energy of 630 Wh kg^{-1}, which is about two times higher than that of traditional Li-ion batteries (~200Wh kg^{-1}). Recently, Fu et al. reported a sandwiched cathode configuration composed of micro-Li_2S powder in between two layers of self-weaving, binder-free carbon nanotube electrodes.[107] A high overpotential was used at the beginning for charging to overcome the energy barrier of micro-Li_2S, because it has a high electronic resistivity and low lithium ion diffusivity. After the first activation, a high capacity of 838 mAh g^{-1} at C/10 was achieved without noticeable overpotential during charge/discharge, which corresponds to 72% of the theoretical capacity of Li_2S. The unique sandwiched electrode architecture for Li_2S cathode facilitates ion and electron transport and traps polysulfides within the positive electrode.

Nano-Li_2S. Zhang et al. reduced the micro-Li_2S to nano-Li_2S by using high-energy ball-milling of commercial micro-Li_2S with carbon black.[108] The high-energy ball-milling reduced the particle size of micro-Li_2S to nano-Li_2S and enhanced its electronic conductivity by building strong bonds between Li_2S and carbon black. The first discharge of the Li_2S-C composite cathode exhibited a high capacity of 1,144 mAh·g^{-1} (normalized to Li_2S), very close to its theoretical maximum (1,166 mAh·g^{-1}). The cycling stability of the Li_2S-C electrodes was further improved by adding multi-walled carbon nanotubes to the nanocomposites, which exhibited a good discharge capacity of 455 mAh·g^{-1} at C/10 after 50 cycles. With high specific energy demonstrated here (~610 Wh·kg^{-1}), the Li_2S-based battery

cell offers promise for the development of high specific energy rechargeable lithium batteries. Recently, Nan et al. synthesized nano-Li_2S spheres with size control for the first time and then applied a chemical vapor deposition method for converting them into stable carbon-coated Li_2S core-shell (Li_2S@C) particles (Fig. 12a).[109, 110] The resulting Li_2S@C particles show a high initial discharge capacity of 972 mAh g^{-1} Li_2S (1,394 mAh g^{-1} S) at the C/5 rate (Fig. 12b), which is due to the protective and conductive carbon shell. Even with no added carbon, a very high Li_2S content (88 wt% of Li_2S) electrode composed of 98 wt% 1μm Li_2S@C spheres and 2 wt% binder shows rather stable cycling performance and not much morphology change after 400 cycles at the C/2 rate.

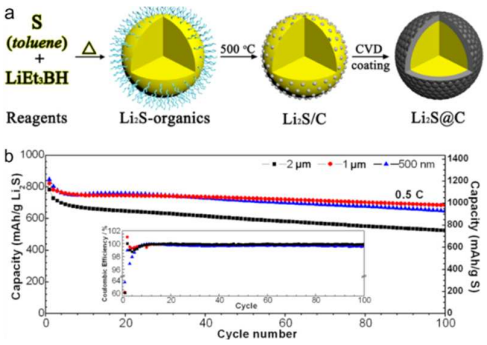

Fig. 12. (a) Schematic of the coating process for the Li_2S@C spheres. (b) Cycling performances of the 2μm, 1μm, and 500nm Li_2S@C particles at the C/2 rate.[109] Reprinted with permission; © 2014 American Chemical Society.

Even for the above great achievements in the sulfur cathode, the polysulfide shuttle is still a big challenge in Li-S cells with low coulombic efficiency unless the lithium anode is passivated. The role of additives in protecting the lithium surface was thoroughly elucidated,[111] which inspire the development of 'catholyte'-type cells where the lithium polysulfides is completely solubilized. Nazar et al. report a strategy based on Ti_4O_7 cathode,[112] an inherently polar, high surface area metallic oxide cathode host, which have the ability to chemically bind polysulfides on the surface and facilitate its reduction to Li_2S. Complementary physical and electrochemical probes demonstrate strong polysulfide/Li_2S binding with this 'sulphiphilic' host and provide experimental evidence for surface-mediated redox chemistry. The practical sulfur mass fraction is up to 70 wt%. The Ti_4O_7/S cathodes provide a discharge capacity of 1,070 mAh g^{-1} and double the capacity retention in comparison to a typical conductive carbon electrode. Stable cycling performance is demonstrated at high rates over 500 cycles. Moreover, the liquid battery design for Li-S cells is also designed based on the catholyte concept, which will be discussed in detail in the section of 4.6.

4.2. Lithium negative electrodes

Long-term cycling of the metallic lithium anode in an organic liquid electrolyte is as important as that of the sulfur positive electrode for practical Li-S cells. Although metallic lithium has a high theoretical capacity of 3,860 mAh g^{-1}, it suffers from drawbacks of dendrite formation and low cycling efficiency. Highly reactive lithium metal electrodes also form an unstable solid electrolyte interphase during cycling, resulting in possible fire hazards and other safety concerns. Surface modifications of

lithium anodes were used to minimize or eliminate dendrite formation, which is more important in Li-S cells than Li-ion cells because of the polysulfide shuttle.[113] In the polysulfide shuttle, sulfur species migrate from the cathode to the anode, leading to the corrosion of the metallic lithium anode and the deposition of insoluble Li_2S_2 and/or Li_2S on the lithium surface. When fully discharged, the discharge product of S (i.e., Li_2S) precipitates from organic electrolytes because of relatively poor solubility. In an attempt to mitigate the parasitic chemical reactions of soluble polysulfides with the lithium anodes, additives to organic liquid electrolytes have been explored.[114-116]

Lithium nitrate ($LiNO_3$) was widely studied for its effectiveness in passivation of the lithium anodes and improving the cyclability of Li-S cells. Aurbach et al. used Fourier transform infrared and X-ray photoelectron spectroscopy to study the effectiveness of $LiNO_3$ on passivation of the lithium metal surface.[117] The components of the electrolyte in this study were 1,3-dioxolane (DOL), lithium bistrifluoromethanesulfone imide (LiTFSI), polysulfide (Li_2S_n), and the $LiNO_3$ additive. The result showed that a passivation layer forms on the surface of the Li electrodes in the presence of $LiNO_3$. This passivation layer consist of Li_xNO_y and Li_xSO_y species, which come from direct reduction of $LiNO_3$ and oxidation of sulfur species by $LiNO_3$, respectively. This passivation layer remarkably diminishes the reduction of polysulfide species by the reactive lithium anode. The coulombic efficiency and cyclability of Li-S cells are dramatically improved.

Phosphorous pentasulfide (P_2S_5), a relatively new additive compared with $LiNO_3$, gained attention for its ability to form a passivation layer as well as increase the solubility of Li_2S. Lin et al. explored the use of P_2S_5 as an additive to the liquid electrolyte.[114] The addition of P_2S_5 to the organic electrolyte led to the formation of a highly protective passivation layer on the metallic lithium surface (Fig. 13a), which functioned similarly to the passivation layer formed using $LiNO_3$ as the additive. This passivation layer prevented the polysulfides from reacting with the metallic Li anode and greatly improved the coulombic and energy efficiencies of the S cathode in cycling. Additionally, P_2S_5 combined with Li_2S to form Li_2S_x/P_2S_5 (x=1) complex, which was soluble in the organic electrolyte tetraethyleneglycol dimethyl ether (TEGDME). Moreover, a series of Li_2S_x/P_2S_5 ($2\leq x\leq 8$) complexes was also found to dissolve well in the organic electrolyte, which greatly promoted the electrochemical reversibility of reactions of sulfur species during cycling (Fig. 13b). The resulting Li-S cells demonstrated high coulombic efficiency of ≥90% and excellent cycling performance; i.e., 70% capacity retention at 900 mAh g^{-1} over 40 cycles at C/10 (Fig. 13c).

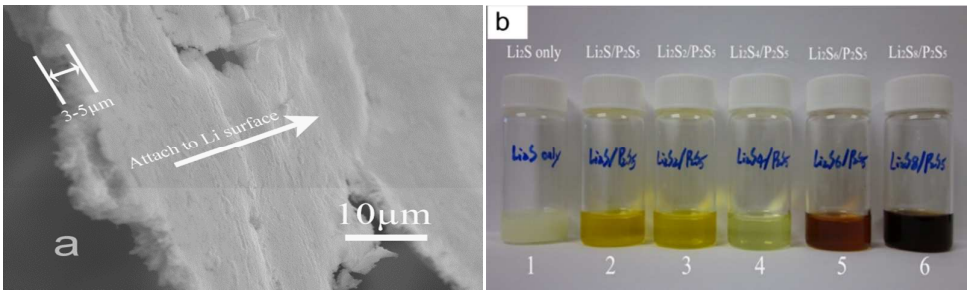

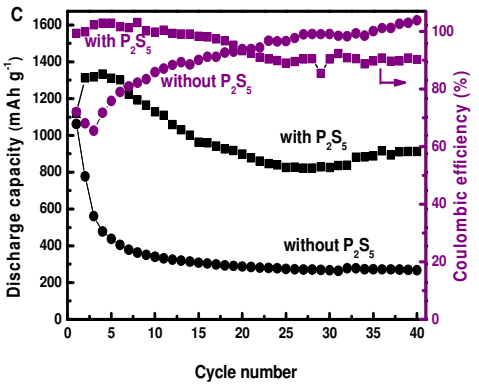

Fig. 13. (a) The cross-section of the passivation layer peeled off from the lithium anode. (b) Insoluble Li_2S (1) and dissolved Li_2S_x/P_2S_5 complexes in TEGDME ([2.] Li_2S/P_2S_5, [3.] Li_2S_2/P_2S_5, [4.] Li_2S_4/P_2S_5, [5.] Li_2S_6/P_2S_5, and [6.] Li_2S_8/P_2S_5). (c) Cycling performance of Li-S batteries with/without P_2S_5.[114] Reprinted with permission; © 2013 WILEY-VCH Verlag GmbH & Co. KGaA, Weinheim.

Though effective by adding additives, the lithium anode still suffers unstable electrodeposition, a consequence to form uneven electrodeposits on the lithium surface with inevitable defects. Nanoscale interfacial engineering or using hybrid lithium anode could be a promising strategy to tackle the intrinsic problems of lithium metal anodes. Recently, Huang et al. reported a design of lithiated graphite and lithium metal as a hybrid anode for Li-S cells.[118] The lithiated graphite was placed in front of the lithium metal and functions as an artificial, self-regulated solid electrolyte interface layer to control undesired electrochemical reactions on lithium during cycling. The resulting Li-S cells deliver capacities of 800 mAh g^{-1} for 400 cycles at a high rate of 1,737mA g^{-1}, with 11% capacity fade and a coulombic efficiency >99% (Fig. 14a). The surface of Li metal harvested from the hybrid electrode remains relatively clean and free of polysulfide deposits (Fig. 14b). Although some polysulfides are deposited on the graphite surface, undesired sulfur contamination is greatly decreased on the Li metal (Fig. 14c). In comparison, the Li anode dissembled from traditional cycled Li-S cells not only has a large amount of sulfur species on Li surface but deeply penetration into bulk Li (Fig. 14d). The hybrid lithium anode controls undesirable surface reactions on lithium and minimize the deleterious side reactions, leading to significant improvement in Li-S performance.

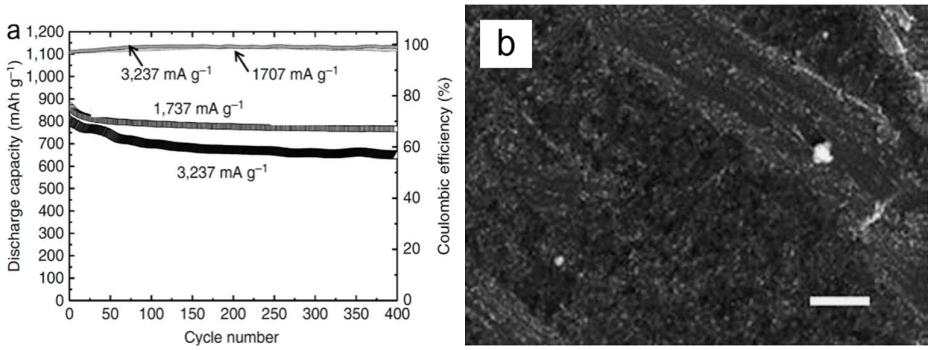

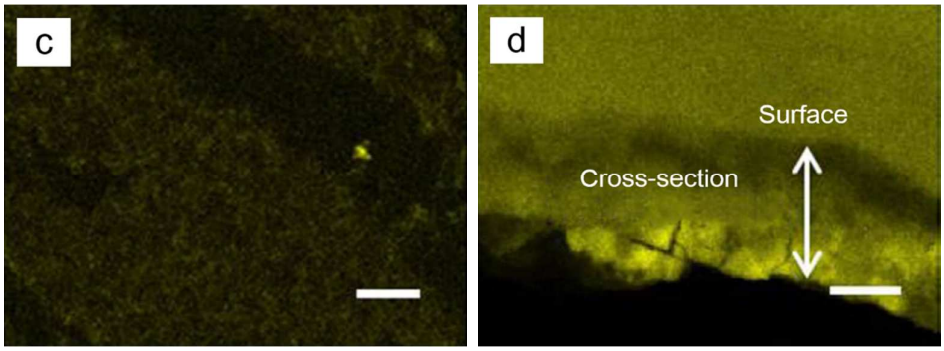

Fig. 14. (a) Long-term cycling behavior and coulombic efficiencies of hybrid Li-S cells at different rates. (b) SEM images of the surface view of Li metal anode from the hybrid anodes after 1,000 cycles. (c) S-elemental mapping of Li metal surface from the hybrid anodes after 1,000 cycles. (d) S-elemental mapping of the Li metal anode from traditional Li-S cells after 1,000 cycles. Reprinted with permission; © 2014 Nature Publishing Group.[118]

4.3. Electrolytes and binders

In addition to the sulfur cathodes and lithium anodes, electrolytes and binders also play significant roles in the cycling stability of Li-S batteries.

Electrolytes. The electrolytes provide effective Li-ion transport between electrodes and work as a charge-transfer medium within the sulfur-containing cathodes. Because of the polysulfide shuttle and the corrosion of lithium anodes, there are special requirements for the electrolytes in Li-S cells; i.e., low viscosity for filling small pores of sulfur cathodes and low solubility of polysulfides. The traditional Li-S batteries use LiTFSI in single or combination of solvents, including 1,3-dioxolane(DOL),[119, 120] dimethoxyethane (DME),[121] tetraethylene glycol dimethyl ether (TEGDME),[122] polyethylene glycol dimethyl ether (PEGDME),[123] tetrahydrofuran (THF),[124] and ionic liquids.[125-127] Prior to this review section, there are good review articles covering electrolytes for Li-S batteries by Scheers et al. and Zhao et al.,[128, 129] respectively. Here, we give some recently developed representatives in novel electrolyte systems for advanced Li-S batteries.

Taking ionic conductivity, viscosity, and salt solubility into consideration, the salt concentration in conventional organic electrolytes is limited to the range of 1-2 mol l^{-1}. By increasing the salt concentration, Hu et al. reported a new class of solvent-in-salt (SIS) electrolytes with ultrahigh salt concentrations and high Li-ion transference numbers.[130] The SIS electrolytes were prepared by dissolving LiTFSI in different volumes of 1DME:1DOL from 1mol l^{-1} (SIS-1#) to 7 mol l^{-1}(SIS-7#). These electrolytes enhanced cycling performance of rechargeable lithium batteries via an effective suppression of lithium dendrite growth. When used in Li-S cells, lithium polysulfide dissolution was greatly inhibited (Fig. 15a). Consequently, a coulombic efficiency nearing 100% and long cycling stability (i.e., high initial capacity of >1,000 mAh g^{-1} with capacity retention of 74%) were achieved after 100 cycles (Fig. 15b).

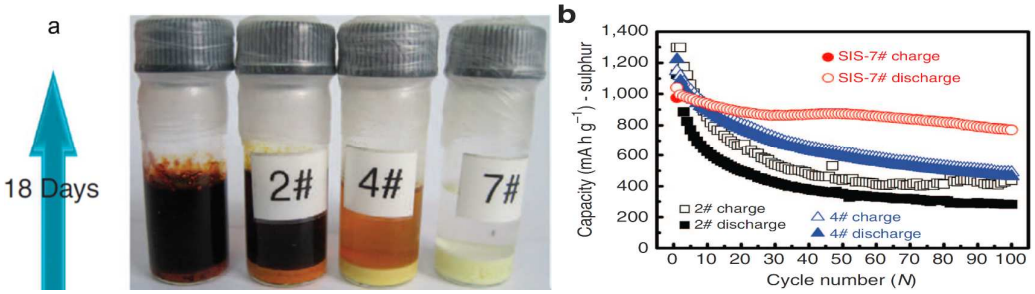

Fig. 15. (a) The color changes of four samples after 18 days with different salt concentrations containing the same amount of Li_2S_8: 0 mol l^{-1}; 2#, 2 mol l^{-1}; 4#, 4 mol l^{-1}; and 7#, 7 mol l^{-1}. (b) Cycling performance of C/S electrodes in electrolytes with different ratios of LiTFSI to 1DOL:1DME (by volume).[130] Reprinted with permission; © 2013 Nature Publishing Group.

Weng et al. also showed good performance of Li-S cells when using partially fluorinated ether electrolytes.[131] Partially fluorinated ethers have superior properties such as low melting point, high oxidation potential, and low flammability, which make them promising alternatives to other organic electrolytes. When used in Li-S cells, the electrochemical performance was greatly enhanced. The Li-S cells delivered an initial discharge capacity of 1,195 mAh $g^{-1}$and a reversible capacity of 836 mAh g^{-1} at the 100th cycle. This was because of the formation of stable thin film on the lithium metal surface introduced by partially fluorinated ether electrolytes, which protected the lithium anode from reacting with polysulfides in the electrolyte. Most recently, Song et al. reported a Li-S cell by employing a cetyltrimethyl ammonium bromide-modified sulfur-graphene oxide nanocomposite cathode in a new formulation of an ionic liquid-based electrolyte.[132] This ionic liquid-based electrolyte consists of 1mM g^{-1} LiTFSI in (n-methyl-(n-butyl) pyrrolidiniumbis(trifluoromethanesulfonyl)imide (PYR_{14}TFSI)/polyethylene glycol dimethyl ether (PEGDME) mixture (1:1, by weight). The Li-S cell was discharged at rates as high as 6C (1C =1,675 mA g^{-1} of S) and charged at rates as high as 3C while still maintaining high specific capacity of 800 $mAhg^{-1}$ of S at 6C. It also showed an excellent cycle life of 1,500 cycles with a high specific capacity of ~740 mAh g^{-1} and a low decay rate of 0.039% per cycle, one of the best cycling performances demonstrated so far. The Li-S cell with lithium metal electrode was cycled with an excellent coulombic efficiency of 96.3% after 1,500 cycles, which also confirmed good performance of this ionic liquid-based electrolyte.

Binders. Binders also play an important role in improving cell performance. A good binder exhibits great adhesion with electrode materials and maintains electrode integrity during cycling.[133] Polyethylene oxide (PEO) and polyvinylidene fluoride (PVDF) are the most commonly used binders; however, they have poor adhesion properties when used in Li-S cells. To address this issue, gelatin was investigated as a water-soluble binder for sulfur-based electrodes.[134-136] Huang et al. reported the improvement in the electrochemical performance of sulfur electrode when using gelatin as the binder.[134] The gelatin binder-sulfur cathode achieved a high initial capacity of 1,132 mAh g^{-1} with capacity retention of 40% after 50 cycles, which was better than using the PEO binder. Recently, Rao et al. reported a new binder using an elastomeric styrene butadiene rubber and carboxy methyl cellulose (CMC).[137] CMC functioned as a thickening agent, which helped with preservation of the electrode integrity during cycling. The subsequent sulfur electrodes exhibited better cycling performance than those using PEO and PVDF binders. Sodium alginate (Na-alginate) was used as an

effective binder for the Si anode in Li-ion batteries.[138] The excellent elasticity and functional groups help in buffering large volume change of the Si anode and assist in building a deformable and stable solid-electrolyte interphase on the Si surface. Bao et al. introduced Na-alginate as a novel binder for the Li-S battery cathode.[139] The electrochemical impedance spectroscopy indicated that the alginate sulfur cathode had lower resistance and better kinetic characteristics than those of the PVDF sulfur cathode. The discharge capacity and the capacity retention rate of Na-alginate sulfur cathode were 508 $mAhg^{-1}$and 65.4% at the 50^{th} cycle with a current density of 335 mA g^{-1}. Compared with the PVDF sulfur cathode, the Na-alginate sulfur cathode showed a remarkably better cycle performance. These results show that the Na-alginate binder has promising potential for Li-S battery applications.

4.4. Interlayers

Porous carbon is used as electron pathways and as traps for dissolved polysulfide species. A new cell configuration developed by Manthiram et al., i.e., a porous carbon interlayer between the separator and cathode disk, effectively improves the electrochemical performance of the Li-S cells.[140-142] For example, Su et al. presented an insertion of an electrolyte-permeable microporous carbon paper between the sulfur cathode and separator (Fig. 16a). As exhibited in Fig. 16b, the cyclability at 1C retains more than 1,000 mAh g^{-1} after 100 cycles with a capacity retention of 85% and an average coulombic efficiency of 97.6%. The charge efficiency of the first two cycles is higher than 100% because of the re-utilization of the sulfur core in the cathode. The carbon interlayer with micropores facilitates the absorption of soluble polysulfides shuttle and makes them reutilized even during long cycles. This novel approach not only simplifies battery processing without elaborate composite syntheses and surface modification, but also improves capacity and cycle life. Under this concept, different conductive materials, such as nickel foam and graphene,[143, 144] also were developed for Li-S cells. Huang et al. developed this strategy by introducing an ion-selective membrane to improve the stability and coulombic efficiency of Li-S cells.[145] The sulfonate-ended perfluoroalkyl ether groups on the ionic separators are connected by pores or channels that are several nanometers in size. These SO^{3-} groups-coated channels allow ion hopping of positively charged species (Li^{+}) but reject hopping of negative ions such as polysulfide anions (S_x^{2-}) because of the coulombic interactions. This cation-selective membrane acts as an electrostatic shield for polysulfide anions and confines the polysulfides on the cathode side. An ultra-low decay rate of 0.08% per cycle is achieved within the initial 500 cycles for this ion-shield membrane. Such an ion-selective membrane is versatile for various electrodes and working conditions, which is promising for construction of high-performance Li-S cells. The importance of the effective separation of lithium and sulfur by carbon film interlayer is confirmed by lithium conductive ceramics. Dominko et al. demonstrate the importance of effective separation between the sulfur cathode and the lithium anode in Li-S batteries.[146] Improved cycling stability is obtained by using commercially available $Li_{1+x+y}Al_xTi_{2-x}Si_yP_{3-y}O_{12}$ membrane as a separator. The sulfur cathode contained 45 wt% of sulfur, and a sulfur loading of 1 mg cm^{-2}. Good cycling stability over 350 cycles with a coulombic efficiency above 99.95% was achieved. The cycling improvement is attributed to the reduced reactivity of long-chain polysulfides with the metallic lithium and to the homogenous distribution of end-discharge products during cycling.

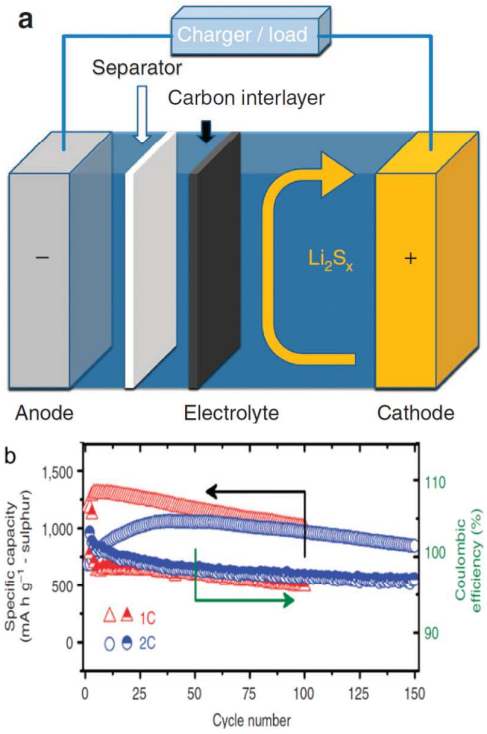

Fig. 16. (a) Schematic configuration of a Li-S cell with a porous carbon interlayer between the sulfur cathode and the separator. (b) Cycle life and coulombic efficiency of the cell with microporous carbon interlay at 1 and 2C.[142] Reprinted with permission; © 2012 Nature Publishing Group.

4.5. Mechanism studies of cathode reactions

The solubility of long chain lithium polysulfides, Li_2S_x ($4 \leq x \leq 8$) formed in the early stages of the discharge cycle and volume expansion of the fully discharged product (i.e., Li_2S) are responsible for morphological change in the sulfur cathode. Thus it is critically important to understand the cycling mechanism and subsequent structural change in the sulfur cathode under a variety of operating conditions.[147] Powerful characterization tools, such as in-situ XRD, X-ray absorption spectra (XAS) and synchrotron-based spectroscopic and scattering techniques are widely used to investigate the degradation mechanisms of Li-S cells and study the structural and compositional changes in detail during battery cycling.[148-150]

The XAS spectra of lithium polysulfides (Li_2S_x) of various chain lengths (x) dissolved in a model solvent were obtained by Pascal et al. from first-principles calculations.[151] The spectra exhibit two main absorption features near S K-edge, which are unambiguously interpreted as a pre-edge near 2,471 eV because of the terminal sulfur atoms at either end of the linear polysulfide dianions and a main-edge near 2,473 eV because of the x-2 internal atoms in the chain (x=8, Fig. 17). An almost linear dependence between the ratio of the peaks and chain length was confirmed without dependence on the delocalized, molecular nature of sulfur atoms. The ratio of the peak area, and not the peak intensities, should be used when attempting to differentiate the polysulfides from XAS when studying reaction mechanism of Li-S cells during cycling.

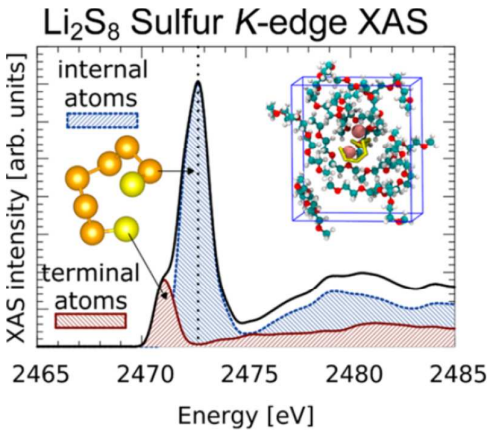

Fig. 17. Schematic illustration of the XAS spectra of Li_2S_x (x=8) S *K*-edge.[151] Reprinted with permission; © 2014 American Chemical Society.

Canas et al. designed a Li-S cell suitable for the study of structural change in the sulfur cathode during cycling using in-situ XRD analysis.[152] The formation of reaction products during charge/discharge was monitored in real time. At the first discharge, the reduction of sulfur species to Li_2S happened at a discharge rate of 300 mA g^{-1}. The formation of Li_2S was first observed at a discharge of 60% in the second discharge plateau at 1.8 V. During the charge cycle, the Li_2S was fully converted back to S_8, however, the sulfur re-crystallized with different structure and smaller particle size. The amount of crystalline S_8 and Li_2S were semi-quantitatively determined by integrated XRD intensity. Moreover, the ex-situ SEM images showed a significant morphological change in the cathode surface during cycling, which was an expected result from the synergistic effect of dissolved Li_2S_x ($4 \leq x \leq 8$) and volume expansion of Li_2S.

Using synchrotron-based transmission X-ray microscopy, Nelson et al. monitored the morphological change in a sulfur electrode in real time during cycling.[153] During discharge, the intensity of crystalline sulfur decreased and entirely disappeared at the end of the first plateau, where long-chain lithium polysulfides formed. At the same time, the particle size decreased and porosity increased because of the dissolution of long-chain lithium polysulfides (Fig. 18a). However, the presence of Li_2S was not observed at the end of discharge, which is contradictory to the in-situ XRD studies on sulfur electrodes mentioned above. During charge, the re-crystallized sulfur reappeared at the end of the charge (Fig. 18b). Most of soluble polysulfides were trapped within the positive electrode during cycling; however, it only takes a small amount of dissolved polysulfides to lead to quick capacity decay. This study highlights the importance of in-situ techniques in determining fundamental mechanisms for battery cycling, which can direct design of Li-S cells with improved performance.

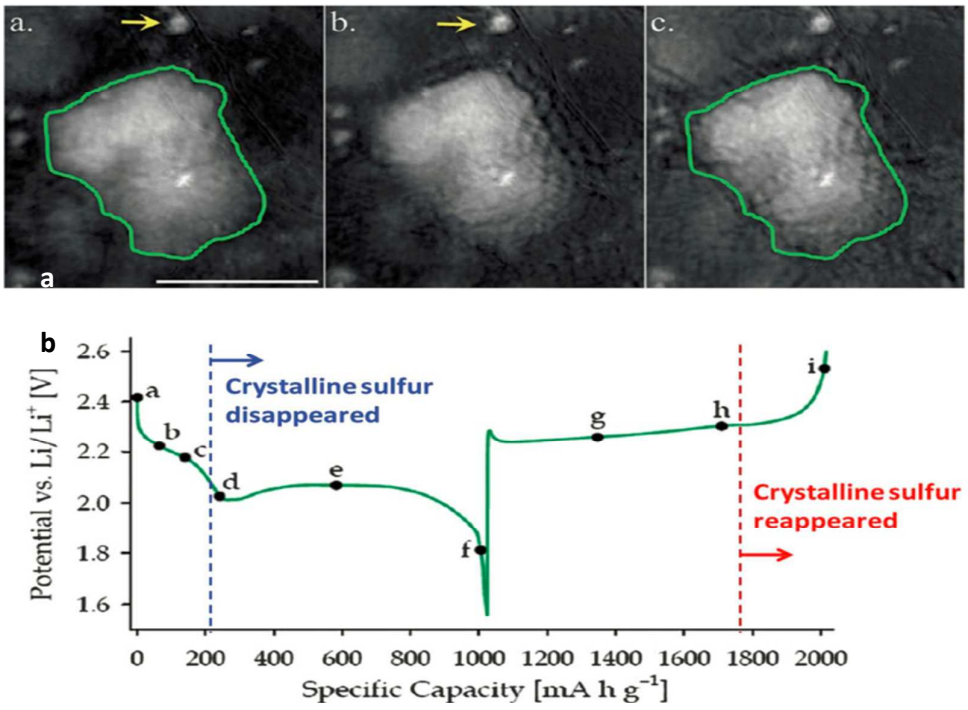

Fig. 18. (a) In situ transmission X-ray microscopy images of a sulfur-carbon cathode during cell operation. (b) The letters along the curve cycle correspond to points in Fig.18a.[153] Reprinted with permission; © 2012 American Chemical Society.

Except for the in-situ XRD and XAS, other techniques such as operando UV-vis, in-situ CV, in-situ impedance, HPLC, XPS,[148, 154-157] was also used to study the cycling mechanism of Li-S batteries. Wagner used the UV-vis spectroscopy to investigate the reduction process of sulfur during cycling.[155] The characteristic absorption bands of sulfur and dilithium sulfide in TEGDME are at 265 and 255 nm, respectively. Reference solutions of polysulfides diminish the band in the UV region with decrease of polysulfide order, which is also observed between 25-75% depth of discharge (DOD). At 425 and 615 nm, absorption bands are identified in the reference polysulfide solutions and also in electrolyte at different DOD. These bands are interpreted as the characteristic bands of S_4^{2-} and S_3^{2-}, and concentration changes of these species are determined semiquantitatively. The highest concentration of polysulfides is found at around 37% DOD. This was confirmed by the results of electrochemical impedance spectroscopy and computer simulations. Barchasz et al. proposed a possible mechanism for sulfur reduction consisting of three steps based on UV and HPLC data (Fig. 19).[148] UV and HPLC data show that long polysulfide chains such as S_8^{2-} and S_6^{2-} are produced during the first reduction step (2.4-2.2 V vs Li/Li^+). The $S_3^{\bullet-}$ radical is produced due to the disproportionation reaction. S_4^{2-} is found during the second reduction step (2.15-2.1 V vs. Li/Li^+), thus pointing out the gradual decrease of the polysulfide chain lengths. Finally, short polysulfide species, such as S_3^{2-}, S_2^{2-}, and S^{2-}, are produced at the end of the reduction process, i.e., between 2.1 and 1.9 V vs. Li/Li^+. The precipitation of the poorly soluble and insulating short polysulfide compounds was also confirmed, thus leading to the positive electrode passivation and explaining the early end of discharge.

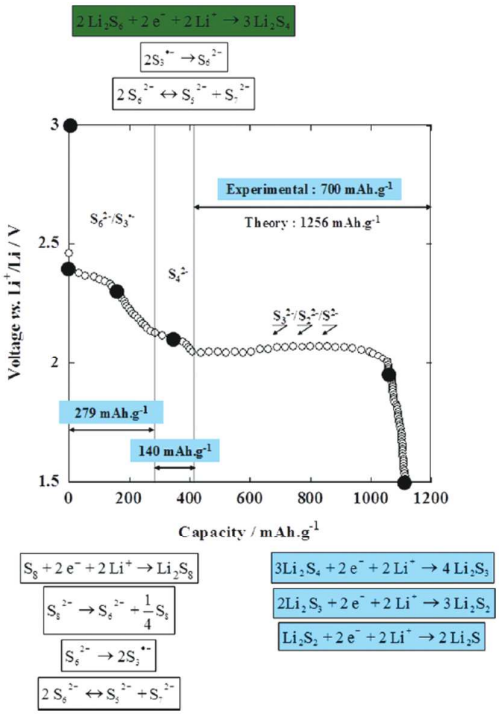

Fig. 19. Proposed sulfur reduction mechanism, involving disproportionation and electrochemical reactions. Major lithium polysulfide compounds are listed on the figure, as well as the specific capacities corresponding to each step.[148] Reprinted with permission; © 2012 American Chemical Society.

4.6. Liquid battery

The need for low-cost efficient energy storage at large-scale capacity facilitates the growth and integration of renewable energy. Liquid rechargeable batteries possess an attractive architecture for such storage due to their ability for large stored energy (the tanks) and power (the stack).[3, 158] Based on dissolved polysulfide species, a liquid sulfur battery was first designed by Rauh et al. in 1979, which supplied a practical energy density of ~300 Wh kg^{-1} using a standard cell design.[159] Recently, a promising new approach of semi-liquid batteries using lithium polysulfide (Li/PS) solutions was developed by Cui et al.[160] In this system, lithium polysulfide of Li_2S_8 in 1:1 DOL/DME and passivated metallic lithium by $LiNO_3$ are used as the catholyte and the anode, respectively. The catholyte is only cycled between sulfur and Li_2S_4, but not to the insoluble Li_2S_2 and Li_2S phases. This inhabits the nucleation and volume change of insoluble Li_2S_2/Li_2S with improved cycle life. This proof-of-concept Li/PS battery has a theoretical energy density of 170 Wh kg^{-1} and 190 Wh L^{-1} based on the mass and volume of the catholyte and lithium. Manthiram et al. also developed high-performance Li/dissolved polysulfide batteries using a sandwich cathode containing a pristine carbon nanofiber current collector filled with polysulfides and a hydrophilic composite upper current collector.[161] The concentration of sulfur in the liquid electrolyte is up to 60 wt% and the sulfur loading is as high 5.5 mg cm^{-2}. Tarascon et al. also designed liquid Li-S cells by drastically deviating from confining approach through a liquid cathode either by dissolving polysulfides within the electrolyte or by placing sulfur powders in contact

with the Li negative electrode. Such a strategy eliminates the detrimental Li_2S formation inside a porous carbon matrix and moreover leads to the formation of a protective SEI layer at the Li electrode. These approaches resulted in greater performance than confinement approaches.[162] More recently, Chiang et al. demonstrated for the first time lithium polysulfide half-flow cells operating in both continuous and intermittent flow battery mode (Fig. 20).[163] Diffusion-limited aggregation of nanoscale conductor particles at ~1 vol% concentration is used to impart mixed electronic-ionic conductivity to redox solutions. This nanoscale network architecture enables cycling of polysulfide solutions deep into insoluble Li_2S_2 and Li_2S phases with good capacity utilization and reversibility.

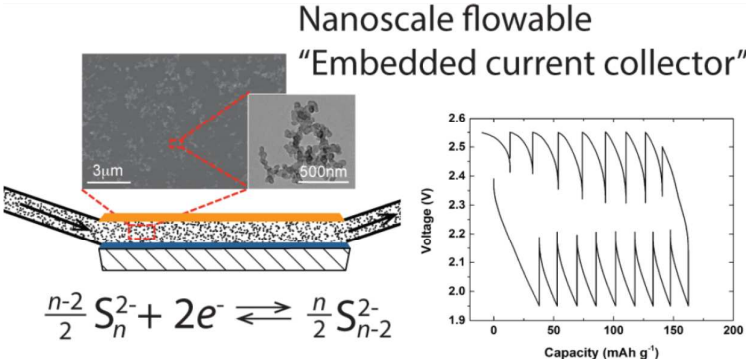

Fig. 20. The schematic of electronically conductive flowing redox electrodes based on nanoscale percolating networks of conductor particles for lithium/polysulfide half-flow cells.[163] Reprinted with permission; © 2014 American Chemical Society.

5. Recently developed solid cells

Though much effort was dedicated to improving the performance of Li-S batteries, the polysulfide shuttle and lithium dendrite formation in organic liquid electrolytes are still tough challenges in traditional Li-S cells. The replacement of liquid electrolytes by solid electrolytes eliminates the polysulfide shuttle and enables stable cycling of metallic lithium anodes.[164, 165] This modification opens the door to game-changing possibilities for Li-S batteries.[166-169] The removal of any liquid component in solid Li-S cells leads to consistent improvements in cycling performance, reliability, and safety for practical application. With the discovery of solid electrolytes with ionic conductivities comparable to that of liquid electrolytes, all-solid rechargeable lithium batteries promise to be the next breakthrough for electric energy storage.[170] However, relatively large volume change of 76% in solid Li-S cells always results in poor cycling performance; hot-press or high-pressure press and binders such as PVDF or PVC were used to buffer the volume change and maintain the contact between the electrodes and the solid electrolyte.[171-173] In this section, we discuss and highlight the most recent breakthroughs in all-solid Li-S cells, including solid electrolytes and electrode materials.

5.1. Solid electrolytes

The electrolyte is the key component of any practical solid cell. A good solid electrolyte must

have an excellent ionic conductivity at room temperature, good compatibility with metallic lithium, and a wide electrochemical window (up to 5 V vs. Li/Li^+). Different kinds of solid electrolytes, including polymer electrolytes,[174-176] thio-LISICON electrolytes,[177] and Li_2S/P_2S_5-based electrolytes,[178, 179] were widely studied for their improvement in ionic conductivity and application in solid lithium batteries.

Polymer electrolytes. The use of polymer electrolytes eliminates any liquid component; as a result, the solid cells prevent the polysulfide shuttle in the traditional Li-S cells and enhance the cycling performance. Polymer electrolytes with specific compositions were designed specifically for desired battery performance. Scrosati et al. reported nanocomposite polymer electrolyte (NCPE) prepared by hot-pressing a poly(ethylene oxide)-lithium triflate ($PEO\text{-}LiCF_3SO_3$) complex membrane containing nano-sized zirconia (ZrO_2) and lithium sulfide (Li_2S).[180] The ionic conductivity of NCPE is on the order of 10^{-4} to 10^{-3} S cm^{-1} at 70 °C and above (Fig. 21a), which results from the mobility of the PEO polymer chain at higher temperatures. When NCPE electrolyte was applied in all-solid Li-S cells, the initial specific capacity of sulfur cathode was 900 mAh g^{-1} (Fig. 21b), and the coulombic efficiency approached 100%. Recently, Liang et al. reported the solid Li-S cell based on polymer electrolyte of $PEO_{18}Li(CF_3SO_2)_2N$-10 wt%SiO_2.[181] The conductivity is 5×10^{-4} S cm^{-1} at 70 °C. Mesoporous carbon sphere with the uniform channels (OMC) was employed as the conductive matrix in the sulfur cathode. The S-OMCs composite showed excellent cycling performance with a reversible discharge capacity of about 800 mAh g^{-1} after 25 cycles at 70 °C. This is because active sulfur is highly dispersed in and contacted with the OMCs matrix and PEO polymer electrolyte has high ionic conductivity at enhanced temperature.

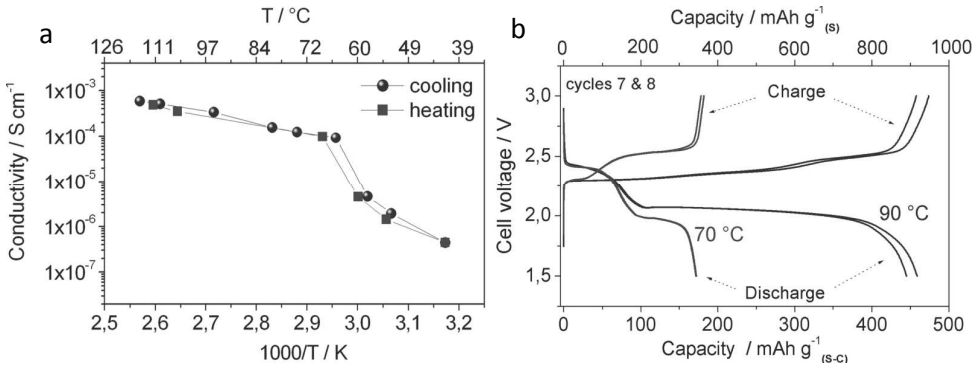

Fig. 21. (a) Conductivity Arrhenius plot of NCPE determined on heating and cooling scans. (b) Charge-discharge profile of the Li/NCPE/S-C solid cell at two temperatures and at C/20 in the range of 1.5-3 V.[180] Reprinted with permission; © 2010 WILEY-VCH Verlag GmbH & Co. KGaA, Weinheim.

Glass-ceramic electrolytes. Thio-LISICON ($Li_{3.25}Ge_{0.25}P_{0.75}S_4$) was synthesized by a solid-state reaction and was used as a solid electrolyte.[177] The thio-LISICON has a high ionic conductivity of ~2×10^{-3} S m^{-1} at room temperature, which is comparable to those of liquid electrolytes. Mesoporous carbon of CMK-3 was used as the conductive framework for the sulfur electrode, which provided high electrical conduction and improved electrode material utilization. The sulfur provided a high reversible capacity and high current charge-discharge characteristics. When the electrode contained 50 wt% sulfur, it showed first discharge capacity of 1,068 mAh g^{-1} with the capacity retention of 70% after 20 cycles. Lithium thiophosphates also were studied intensively as promising solid electrolytes for all-solid

lithium batteries. Recently, the partial substitution of phosphorus (P) atoms by germanium (Ge) atoms in lithium thiophosphate showed an unprecedented high ionic conductivity of 1.2×10^{-2} S cm^{-1}, a value comparable to those of the liquid electrolytes used in Li-ion batteries.[170] Unfortunately, the Ge doping sacrifices the chemical compatibility of the lithium thiophosphate with metallic lithium. To overcome this issue, Liu et al. created nanostructured Li_3PS_4, which showed an enhancement of 3 orders of magnitude in room temperature Li-ion conductivity of the bulk lithium thiophosphate (Fig. 22).[182] Both the reduction of dimensions to a nano-sized framework and high surface-to-bulk ratio of the nanoporous structures contributed to the enhancement of ionic conductivity. Nanostructured Li_3PS_4 presented a wide electrochemical window (i.e., 5V) and superior chemical stability against metallic lithium. This nanostructured Li_3PS_4 was successfully applied as a novel solid electrolyte in solid Li-S cells,[173, 183] which are discussed in detail in the following section.

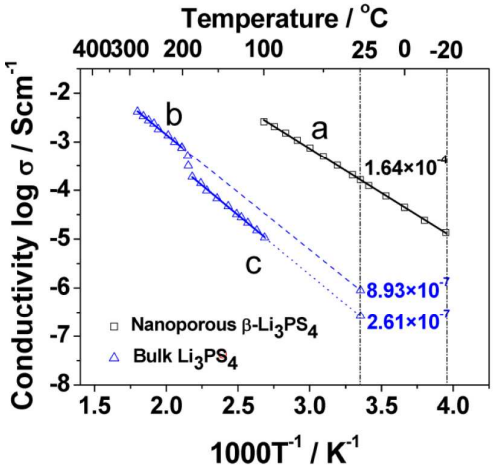

Fig. 22. Arrhenius plots for nanoporous β-Li_3PS_4 (line a), bulk β-Li_3PS_4 (line b), and bulk γ-Li_3PS_4 (line c).[182] Reprinted with permission; © 2013 American Chemical Society.

5.2. Electrode design

As in conventional Li-S batteries, seamless transport of ions and transfer of electrons are basic requirements for all-solid Li-S batteries. To attain good cycling performance, all-solid Li-S batteries have to overcome the poor electronic and ionic conductivities of the sulfur cathode. The sulfur cathode for all-solid batteries was fabricated primarily by high-energy mixing or ball-milling sulfur with conductive carbons and solid electrolytes.[184, 185] The electronic conductivity of the sulfur cathode has been improved by the addition of carbon to the cathode; however, the ionic conductivity of sulfur cannot be significantly improved by the simple mixing of solid electrolytes with sulfur. A great enhancement in the ionic conductivity of sulfur-based cathode is vitally important for excellent performance of all-solid Li-S cells.

Recently, Lin et al. presented a facile method for synthesizing a lithium sulfide (Li_2S) cathode with an enhancement in the ionic conductivity of 6 orders of magnitude.[173] As mentioned above,Li_2S has a favorably high theoretical capacity of 1,166 mAh g^{-1} and can be used as a pre-lithiated cathode to avoid the direct use of metallic lithium as the anode. However, the ionic conductivity of bulk Li_2S is

relatively low (10^{-13} S cm^{-1}), which prevents it from acting as an effective cathode material for all-solid Li-S cells. Nanostructured lithium sulfide (NanoLi_2S), prepared by reacting elemental S with lithium triethylborohydride ($LiEt_3BH$), had an ionic conductivity 2 orders of magnitude greater than that of the bulk Li_2S. The reduced particle size and increased defects of the NanoLi_2S account for the boost in the ionic conductivity. The ionic conductivity of NanoLi_2S was further improved by 4 orders of magnitude by coating with lithium phosphorus sulfide (Li_3PS_4), thus rendering the material a lithium superionic sulfide (LSS) (Fig. 23a). Excellent cycling performance was demonstrated (Fig. 23b) using the LSS and NanoLi_2S as cathode materials for all-solid Li-S batteries at 60 °C. The loading of NanoLi_2S is about 50 wt% in the electrode. The LSS cathode had an initial discharge capacity of 848 mAh g^{-1}, indicative of a 73% utilization of Li_2S. The discharge capacity stabilized at 594 mAh g^{-1} after 100 cycles, and the coulombic efficiency of 100% was observed after 30 cycles. The polysulfide shuttle has been completely eliminated in the all-solid Li-S batteries. The voltage profiles of the NanoLi_2S and LSS are shown in Fig. 23c. Unlike the two-plateau feature in the voltage profile of conventional Li-S cells with liquid electrolytes, only one plateau was observed in the all-solid Li-S cells. The one plateau confirms that unlike the phase transition from solid to liquid phase in liquid cells, there is no phase change during cycling in all-solid Li-S cells.

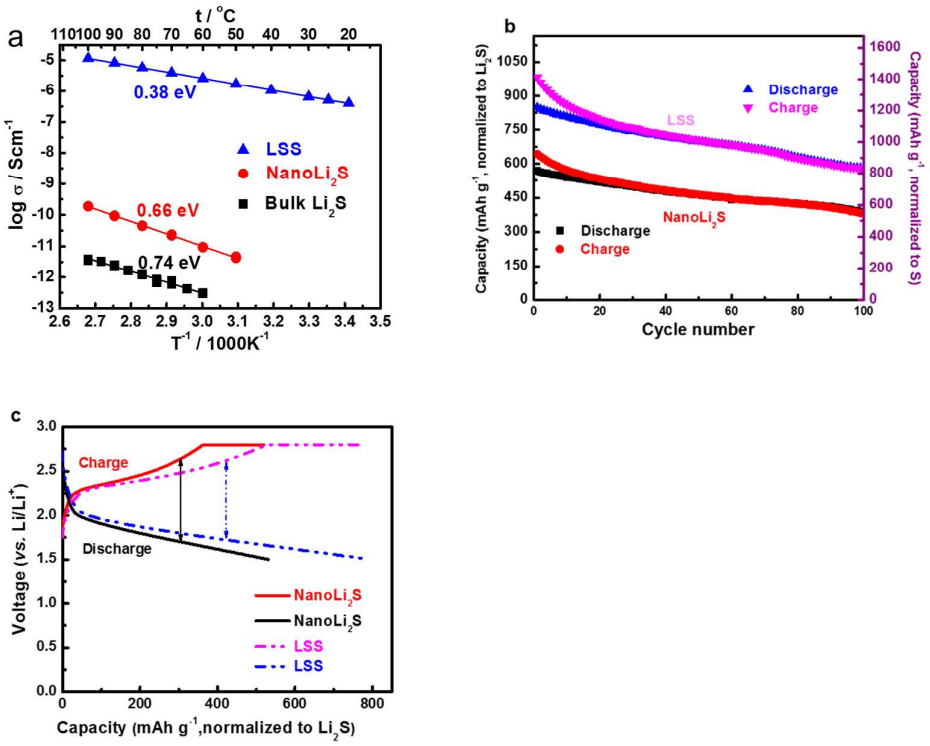

Fig. 23. (a) Temperature dependency of ionic conductivities of the bulk Li_2S, NanoLi_2S, and LSS. (b) The cycling performance of NanoLi_2S and LSS as the cathode materials for all-solid Li-S cells at 60 °C at C/10. (c) Representative voltage profiles of NanoLi_2S and LSS.[173] Reprinted with permission; © 2013 American Chemical Society.

Lin et al. further reported the first series of sulfur-rich compounds, i.e., lithium polysulfidophosphate (LPSP), with high ionic conductivities and excellent electrochemical reversibility for all-solid Li-S batteries.[183] These sulfur-rich compounds were prepared by reacting sulfur with lithium thiophosphate (Li_3PS_4) in THF. Polysulfidophosphate anions were formed through the formation of S-S single bonds at the negatively charged terminal sulfur atoms of PS_4^{3-}. The reaction products of LPSP have a general formula of Li_3PS_{4+n} (0<n<9). The n in the formula represents the number of S-S bonds in the LPSP molecule, which was confirmed by both XRD and Raman spectra. These LPSP compounds are Li-ion conductors with room-temperature ionic conductivity in the range of 10^{-4} to 10^{-6} S cm^{-1}, depending on the number of sulfur atoms. For example, if n=5, the ionic conductivity of Li_3PS_{4+5} is 3.0×10^{-5} S cm^{-1}, which is about 8 orders of magnitude higher than that of bulk Li_2S (Fig. 24a). Excellent cyclability was demonstrated using the Li_3PS_{4+5} cathode for all-solid Li-S cells, when the sulphur loading is in the range of 0.2-0.5 mg cm^{-2}. The cathode showed an initial discharge capacity of 1,272 mAh g^{-1} (based on the incorporated sulfur content, Fig. 24b) with 100% coulombic efficiency after a few initial cycles at room temperature. Even better cycling performance was observed at 60°C. The initial capacity was >1,400 mAh g^{-1}, and a high capacity of 1,200 mAh g^{-1} was maintained after 300 cycles. This observation confirmed that the LPSP has an extremely stable cycling performance. The improved cycling performance was attributed to the increased ionic conductivity of the sulfur-rich cathode and the elimination of the polysulfide shuttle when using an all-solid cell design. A salient characteristic of LPSP is its excellent compatibility with the solid electrolyte; i.e. nanostructured β-Li_3PS_4. A low interfacial resistance at the cathode/solid electrolytes interface is a prerequisite of all-solid Li-S cells. A good rate performance at 60 °C was also shown in LPSP-based Li-S cell. The cell had a capacity over 1,200 mAh g^{-1} at C/10 and showed a reversible capacity of 735 mAh g^{-1} at 2C after 50 cycles at various rates. Further cycling at a low rate of C/10 brought it back to a reversible capacity of 1,200 mAh g^{-1}.

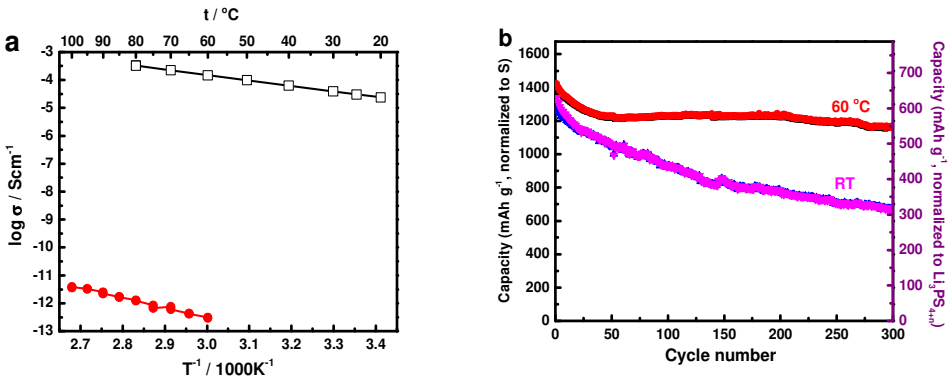

Fig. 24. (a) Temperature dependency of ionic conductivity of lithium polysulfidophosphates (Li_3PS_{4+5}) and (□, Ea=0.37 eV) and Li_2S (●, Ea=0.74 eV). (b) The cycling performance of Li_3PS_{4+5} at the rate of C/10 at room temperature and 60°C (pink/red charge, black/blue discharge).[183] Reprinted with permission; © 2013 WILEY-VCH Verlag GmbH & Co. KGaA, Weinheim.

Although sulfur cathodes in all-solid cells with enhanced ionic conductivities demonstrated excellent cycling performance, further improvements on all-solid Li-S batteries need to be conducted for practical applications. For examples, the sulfur loading needs to be increased to a few mg cm^{-2}, and

all-solid Li-S cells need to be cycled at room temperature at the high C rate such as 2C.

6. Conclusions and perspectives

Though promising, there are still tough challenges associated with the traditional Li-S cells, including the insulating properties of sulfur species and the polysulfide shuttle associated with the sulfur cathode and the dendrite formation and safety concerns associated with the lithium anode. In the past few years, significant efforts have been dedicated to the study of each component in traditional Li-S liquid cells for improved cyclability, including the sulfur positive electrodes, the lithium negative electrodes, and the electrolytes and binders. Various structured materials, such as carbon-sulfur composites, polymer-sulfur composites, and nanostructured Li_2S, have been designed to overcome the problems of the traditional Li-S cells and, thus, dramatically enhance capacity, improve coulombic efficiency, and prolong cycle life. The reaction mechanisms have been researched by monitoring the compositional and morphological changes in the electrodes in real time using in-situ characterization techniques, including in-situ XRD, XAS as well as recently developed technologies such as in-situ impedance, CV, operando UV-vis spectroscopy, and HPLC et al. These advanced developments present promising prospects of practical Li-S batteries.

The research for future directions on the exploration of advanced Li-S batteries with commercially available possibility are summarized as follows: (1) Though there have been many effective protections for the dissolution of sulfur cathode, new barrier materials or surface modification on the sulfur cathode that can lead to the final commercialization of Li-S batteries are still expected to be designed; (2) For the commercialization, the improved active sulfur loading in the cathode is needed for higher energy density; (3) The electrochemical mechanisms of the Li-S cells are still unclear and even controversial, it would be better to combine experimental with modeling and simulation for a deeper and broader understanding of reaction mechanisms; (4) A more reliable electrolyte compositions or good additives need be explored to control the polysulfide dissolution and to solve the safety concerns for metallic lithium anodes; (5) The employment of Li_2S rather than S as the cathode for metallic lithium-free anode, and the replacement of the lithium anode with high-capacity anodes such as Si or Sn; (6) Novel cell configuration design, such as the effective interlayer or the lithium ionic conductor barrier, for high performance Li-S batteries, however, special attention should be paid to the energy density of the whole cell when taking this new component into consideration; (7) The usage of catholyte for the applications in liquid batteries such as semi-solid batteries, semi-liquid batteries, and redox flow batteries.

With the emergence of solid electrolytes with ionic conductivities comparable to that of liquid electrolytes, the all-solid Li-S batteries promise to be the next breakthrough for electric energy storage. The utilization of solid electrolytes in Li-S batteries alters the fundamental problems of traditional Li-S batteries: the replacement of liquid electrolytes by solid electrolyte eliminates the polysulfide shuttle and enables high-energy Li-S chemistry with an intrinsically safe cell design. Many advanced solid electrolytes with good ionic conductivity, such as polymer electrolytes and glass-ceramic solid electrolytes, were synthesized for application in all-solid Li-S cells. New electrode materials with high ionic conductivity, including NanoLi_2S and lithium polysulfidophosphate, also were discovered.

Nevertheless, several issues need to be explored for the possible application of all-solid Li-S batteries: (1) Novel solid electrolytes should be designed because their ionic conductivities are

generally too low to meet the required current density at room temperature; (2) Though some Li-ion conducting materials have reasonable ionic conductivity at room temperature, their electrochemical windows and compatibility with metallic lithium should be improved; (3) New families of electrode materials with excellent ionic conductivity and electrochemical reversibility should be synthesized; (4) Interfacial resistance within the electrode and between the electrolyte and electrode should be reduced for practical application; (5) The techniques such as in-situ XRD, XAS as well as in-situ impedance, CV, and operando UV-vis spectroscopy, should be used to studies the interfacial change within the electrode and between the electrolyte and electrolyte; (6) Modeling and simulation should be also needed to predict the interfacial change and guide the research on the electrode and electrolyte for all-solid cells, (7) The loading of sulfur cathode should be increased and the thickness of the solid electrolyte layer should be decreased for good energy density and excellent cyclability; and (8) The rate performance of solid cells at room temperature should be increased.

In summary, as the most promising candidate for the application in the electrification of vehicles, Li-S batteries can supply theoretical energy density five times higher than that of Li-ion batteries. With great interest and extensive research in Li-S cells, there have been significant progresses in improving performance and understanding mechanisms of both traditional liquid and recent all-solid Li-S batteries. We believe that with continued studies by the battery community, all-solid Li-S batteries could be a next-generation breakthrough in advanced energy storage for large-scale grids and vehicular transportation.

Acknowledgements

This work was sponsored by the Division of Materials Sciences and Engineering, Office of Basic Energy Sciences, US Department of Energy (DOE).

References

1 M. I. Hoffert, K. Caldeira, G. Benford, D. R. Criswell, C. Green, H. Herzog, A. K. Jain, H. S. Kheshgi, K. S. Lackner, J. S. Lewis, H. D. Lightfoot, W. Manheimer, J. C. Mankins, M. E. Mauel, L. J. Perkins, M. E. Schlesinger, T. Volk and T. M. L. Wigley, *Science*, 2002, **298**, 981.

2 L. W. Ji, Z. Lin, M. Alcoutlabi and X. W. Zhang, *Energy Environ. Sci.*, 2011, **4**, 2682.

3 B. Dunn, H. Kamath and J. M. Tarascon, *Science*, 2011, **334**, 928.

4 J. M. Tarascon and M. Armand, *Nature*, 2001, **414**, 359.

5 A. S. Arico, P. Bruce, B. Scrosati, J. M. Tarascon and W. Van Schalkwijk, *Nat. Mater.*, 2005, **4**, 366.

6 L. W. Ji, Z. Lin, M. Alcoutlabi, O. Toprakci, Y. F. Yao, G. J. Xu, S. L. Li and X. W. Zhang, *Rsc Adv.*, 2012, **2**, 192.

7 B. K. Guo, Y. Li, Y. F. Yao, Z. Lin, L. W. Ji, G. J. Xu, Y. Z. Liang, Q. Shi and X. W. Zhang, *Solid State Ionics*, 2011, **204**, 61.

8 P. G. Bruce, L. J. Hardwick and K. M. Abraham, *MRS Bull.*, 2011, **36**, 506.

9 E. J. Cairns and Shimotak.H, *Science*, 1969, **164**, 1347.

10 S. Evers and L. F. Nazar, *Acc. Chem. Res.*, 2013, **46**, 1135.

11 Y. X. Yin, S. Xin, Y. G. Guo and L. J. Wan, *Angew. Chem. Int. Edit.*, 2013, **52**, 13186.

12 A. Manthiram, Y. Fu, S.-H. Chung, C. Zu and Y.-S. Su, *Chem. Rev.*, 2014.

13 Y. Yang, G. Y. Zheng and Y. Cui, *Chem. Soc. Rev.*, 2013, **42**, 3018.

14 B. Scrosati and J. Garche, *J. Power Sources*, 2010, **195**, 2419.

15 M. Barghamadi, A. Kapoor and C. Wen, *J. Electrochem. Soc.*, 2013, **160**, A1256.

16 M. K. Song, E. J. Cairns and Y. G. Zhang, *Nanoscale*, 2013, **5**, 2186.

17 G. Y. Zheng, Q. F. Zhang, J. J. Cha, Y. Yang, W. Y. Li, Z. W. Seh and Y. Cui, *Nano Lett.*, 2013, **13**, 1265.

18 T. Q. Lin, Y. F. Tang, Y. M. Wang, H. Bi, Z. Q. Liu, F. Q. Huang, X. M. Xie and M. H. Jiang, *Energ Environ Sci*, 2013, **6**, 1283.

19 C. F. Zhang, H. B. Wu, C. Z. Yuan, Z. P. Guo and X. W. Lou, *Angew. Chem.-Int. Edit.*, 2012, **51**, 9592.

20 S. E. Cheon, K. S. Ko, J. H. Cho, S. W. Kim, E. Y. Chin and H. T. Kim, *J. Electrochem. Soc.*, 2003, **150**, A796.

21 S. E. Cheon, K. S. Ko, J. H. Cho, S. W. Kim, E. Y. Chin and H. T. Kim, *J. Electrochem. Soc.*, 2003, **150**, A800.

22 Y. V. Mikhaylik and J. R. Akridge, *J. Electrochem. Soc.*, 2004, **151**, A1969.

23 E. Peled, A. Gorenshtein, M. Segal and Y. Sternberg, *J. Power Sources*, 1989, **26**, 269.

24 W. K. Wang, Z. B. Yu, K. G. Yuan, A. B. Wang and Y. S. Yang, *Prog. Chem.*, 2011, **23**, 540.

25 A. Manthiram, Y. Z. Fu and Y. S. Su, *Accounts Chem. Res.*, 2013, **46**, 1125.

26 H. S. Ryu, H. J. Ahn, K. W. Kim, J. H. Ahn, J. Y. Lee and E. J. Cairns, *J. Power Sources*, 2005, **140**, 365.

27 H. S. Ryu, H. J. Ahn, K. W. Kim, J. H. Ahn, K. K. Cho and T. H. Nam, *Electrochim. Acta*, 2006, **52**, 1563.

28 M. Q. Zhao, X. F. Liu, Q. Zhang, G. L. Tian, J. Q. Huang, W. C. Zhu and F. Wei, *ACS Nano*, 2012, **6**, 10759.

29 Y. Z. Fu, Y. S. Su and A. Manthiram, *Angew. Chem. Int. Edit.*, 2013, **52**, 6930.

30 J. L. Wang, Z. D. Yao, C. W. Monroe, J. Yang and Y. Nuli, *Adv. Funct. Mater.*, 2013, **23**, 1194.
31 J. C. Guo, Z. C. Yang, Y. C. Yu, H. D. Abruna and L. A. Archer, *J. Am. Chem. Soc.*, 2013, **135**, 763.
32 W. Y. Li, G. Y. Zheng, Y. Yang, Z. W. Seh, N. Liu and Y. Cui, *Proc. Natl. Acad. Sci. U. S. A.*, 2013, **110**, 7148.
33 S. C. Wei, H. Zhang, Y. Q. Huang, W. K. Wang, Y. Z. Xia and Z. B. Yu, *Energy Environ. Sci.*, 2011, **4**, 736.
34 J. Shim, K. A. Striebel and E. J. Cairns, *J. Electrochem. Soc.*, 2002, **149**, A1321.
35 X. L. Ji, K. T. Lee and L. F. Nazar, *Nat. Mater.*, 2009, **8**, 500.
36 G. L. Xu, Y. F. Xu, J. C. Fang, X. X. Peng, F. Fu, L. Huang, J. T. Li and S. G. Sun, *Acs Appl. Mater. Inter.*, 2013, **5**, 10782.
37 L. H. Yu, N. Brun, K. Sakaushi, J. Eckert and M. M. Titirici, *Carbon*, 2013, **61**, 245.
38 K. Xi, S. Cao, X. Y. Peng, C. Ducati, R. V. Kumar and A. K. Cheetham, *Chem. Commun.*, 2013, **49**, 2192.
39 X. F. Wang, X. P. Fang, X. W. Guo, Z. X. Wang and L. Q. Chen, *Electrochim. Acta*, 2013, **97**, 238.
40 X. Y. Tao, X. R. Chen, Y. Xia, H. Huang, Y. P. Gan, R. Wu, F. Chen and W. K. Zhang, *J. Mater. Chem. A*, 2013, **1**, 3295.
41 D. W. Wang, Q. C. Zeng, G. M. Zhou, L. C. Yin, F. Li, H. M. Cheng, I. R. Gentle and G. Q. M. Lu, *J. Mater. Chem. A*, 2013, **1**, 9382.
42 H. Ye, Y. X. Yin, S. Xin and Y. G. Guo, *J. Mater. Chem. A*, 2013, **1**, 6602.
43 S. R. Zhao, C. M. Li, W. K. Wang, H. Zhang, M. Y. Gao, X. Xiong, A. B. Wang, K. G. Yuan, Y. Q. Huang and F. Wang, *J. Mater. Chem. A*, 2013, **1**, 3334.
44 T. H. Hwang, D. S. Jung, J. S. Kim, B. G. Kim and J. W. Choi, *Nano Lett.*, 2013, **13**, 4532.
45 S. T. Lu, Y. W. Cheng, X. H. Wu and J. Liu, *Nano Lett.*, 2013, **13**, 2485.
46 M. S. Park, J. S. Yu, K. J. Kim, G. Jeong, J. H. Kim, T. Yim, Y. N. Jo, U. Hwang, S. Kang, T. Woo, H. Kim and Y. J. Kim, *Rsc Adv.*, 2013, **3**, 11774.
47 X. Yang, L. Zhang, F. Zhang, Y. Huang and Y. S. Chen, *Acs Nano*, 2014, **8**, 5208.
48 X. Z. Ma, B. Jin, P. M. Xin and H. H. Wang, *Appl. Surf. Sci.*, 2014, **307**, 346.
49 G. He, B. Mandlmeier, J. Schuster, L. F. Nazar and T. Bein, *Chem. Mater.*, 2014, **26**, 3879.
50 B. Ding, C. Z. Yuan, L. F. Shen, G. Y. Xu, P. Nie and X. G. Zhang, *Chem. Euro. J.*, 2013, **19**, 1013.
51 B. Wang, Y. F. Wen, D. L. Ye, H. Yu, B. Sun, G. X. Wang, D. Hulicova-Jurcakova and L. Z. Wang, *Chem. Euro. J.*, 2014, **20**, 5224.
52 J. L. Wang, L. C. Yin, H. Jia, H. T. Yu, Y. S. He, J. Yang and C. W. Monroe, *ChemSusChem*, 2014, **7**, 563.
53 S. H. Chung and A. Manthiram, *Electrochem. Commun.*, 2014, **38**, 91.
54 L. Zhou, X. J. Lin, T. Huang and A. S. Yu, *Electrochim. Acta*, 2014, **116**, 210.
55 J. Q. Huang, H. J. Peng, X. Y. Liu, J. Q. Nie, X. B. Cheng, Q. Zhang and F. Wei, *J. Mater. Chem. A*, 2014, **2**, 10869.
56 Y. H. Qu, Z. A. Zhang, X. W. Wang, Y. Q. Lai, Y. X. Liu and J. Li, *J. Mater. Chem. A*, 2013, **1**, 14306.
57 K. K. Jin, X. F. Zhou, L. Z. Zhang, X. Xin, G. H. Wan and Z. P. Liu, *J. Phys. Chem. C*, 2013, **117**, 21112.
58 X. B. Cheng, J. Q. Huang, Q. Zhang, H. J. Peng, M. Q. Zhao and F. Wei, *Nano Energy*, 2014, **4**,

65.
59 N. Brun, K. Sakaushi, L. H. Yu, L. Giebeler, J. Eckert and M. M. Titirici, *Phys. Chem. Chem. Phys.*, 2013, **15**, 6080.
60 S. T. Lu, Y. Chen, X. H. Wu, Z. D. Wang, L. Y. Lv, W. Qin and L. X. Jiang, *Rsc Adv.*, 2014, **4**, 18052.
61 J. J. Tang, J. Yang and X. Y. Zhou, *Rsc Adv.*, 2013, **3**, 16936.
62 D. Chen, L. H. Tang and J. H. Li, *Chem. Soc. Rev.*, 2010, **39**, 3157.
63 S. Flandrois and B. Simon, *Carbon*, 1999, **37**, 165.
64 S. Xin, L. Gu, N. H. Zhao, Y. X. Yin, L. J. Zhou, Y. G. Guo and L. J. Wan, *J. Am. Chem. Soc.*, 2012, **134**, 18510.
65 X. L. Li, Y. L. Cao, W. Qi, L. V. Saraf, J. Xiao, Z. M. Nie, J. Mietek, J. G. Zhang, B. Schwenzer and J. Liu, *J. Mater. Chem. A*, 2011, **21**, 16603.
66 C. D. Liang, N. J. Dudney and J. Y. Howe, *Chem. Mater.*, 2009, **21**, 4724.
67 J. Schuster, G. He, B. Mandlmeier, T. Yim, K. T. Lee, T. Bein and L. F. Nazar, *Angew. Chem. Int. Edit.*, 2012, **51**, 3591.
68 G. Y. Xu, B. Ding, P. Nie, L. F. Shen, J. Wang and X. G. Zhang, *Chem. Euro. J.*, 2013, **19**, 12306.
69 J. C. Guo, Y. H. Xu and C. S. Wang, *Nano Lett.*, 2011, **11**, 4288.
70 Y. S. Yun, V. D. Le, H. Kim, S. J. Chang, S. J. Baek, S. Park, B. H. Kim, Y. H. Kim, K. Kang and H. J. Jin, *J. Power Sources*, 2014, **262**, 79.
71 G. M. Zhou, S. F. Pei, L. Li, D. W. Wang, S. G. Wang, K. Huang, L. C. Yin, F. Li and H. M. Cheng, *Adv. Mater.*, 2014, **26**, 625.
72 J. P. Rong, M. Y. Ge, X. Fang and C. W. Zhou, *Nano Lett.*, 2014, **14**, 473.
73 L. W. Ji, M. M. Rao, H. M. Zheng, L. Zhang, Y. C. Li, W. H. Duan, J. H. Guo, E. J. Cairns and Y. G. Zhang, *J. Am. Chem. Soc.*, 2011, **133**, 18522.
74 J. Q. Huang, X. F. Liu, Q. Zhang, C. M. Chen, M. Q. Zhao, S. M. Zhang, W. C. Zhu, W. Z. Qian and F. Wei, *Nano Energy*, 2013, **2**, 314.
75 H. J. Peng, J. Q. Huang, M. Q. Zhao, Q. Zhang, X. B. Cheng, X. Y. Liu, W. Z. Qian and F. Wei, *Adv. Funct. Mater.*, 2014, **24**, 2772.
76 Y. Zhao, W. Wu, J. Li, Z. Xu and L. Guan, *Adv. Mater.*, 2014, **26**, 5113.
77 K. Xi, P. R. Kidambi, R. J. Chen, C. L. Gao, X. Y. Peng, C. Ducati, S. Hofmann and R. V. Kumar, *Nanoscale*, 2014, **6**, 5746.
78 Q. Li, Z. A. Zhang, Z. P. Guo, Y. Q. Lai, K. Zhang and J. Li, *Carbon*, 2014, **78**, 1.
79 S. Q. Chen, X. D. Huang, H. Liu, B. Sun, W. K. Yeoh, K. F. Li, J. Q. Zhang and G. X. Wang, *Adv. Energy Mater.*, 2014, **4**, 9.
80 W. Zhou, X. Xiao, M. Cai and L. Yang, *Nano Lett.*, 2014, **14**, 5250.
81 L. F. Xiao, Y. L. Cao, J. Xiao, B. Schwenzer, M. H. Engelhard, L. V. Saraf, Z. M. Nie, G. J. Exarhos and J. Liu, *Adv. Mater.*, 2012, **24**, 1176.
82 F. Wu, J. Z. Chen, R. J. Chen, S. X. Wu, L. Li, S. Chen and T. Zhao, *J. Phys. Chem. C*, 2011, **115**, 6057.
83 L. C. Yin, J. L. Wang, J. Yang and Y. N. Nuli, *J. Mater. Chem.*, 2011, **21**, 6807.
84 G. C. Li, G. R. Li, S. H. Ye and X. P. Gao, *Adv. Energy Mater.*, 2012, **2**, 1238.
85 W. D. Zhou, Y. C. Yu, H. Chen, F. J. DiSalvo and H. D. Abruna, *J. Am. Chem. Soc.*, 2013, **135**, 16736.
86 G. Q. Ma, Z. Y. Wen, J. Jin, Y. Lu, X. W. Wu, C. Liu and C. H. Chen, *Rsc Adv.*, 2014, **4**, 21612.

87 Y. Z. Fu and A. Manthiram, *Chem. Mater.*, 2012, **24**, 3081.

88 L. Duan, J. C. Lu, W. Y. Liu, P. Huang, W. S. Wang and Z. C. Liu, *Colloid Surface A*, 2012, **414**, 98.

89 Y. Yang, G. H. Yu, J. J. Cha, H. Wu, M. Vosgueritchian, Y. Yao, Z. A. Bao and Y. Cui, *Acs Nano*, 2011, **5**, 9187.

90 Z. H. Wang, Y. L. Chen, V. Battaglia and G. Liu, *J. Mater. Res.*, 2014, **29**, 1027.

91 J. L. Wang, J. Yang, J. Y. Xie and N. X. Xu, *Adv. Mater.*, 2002, **14**, 963.

92 Y. G. Zhang, Y. Zhao, Z. Bakenov, D. Gosselink and P. Chen, *J. Solid State Electrochem.*, 2014, **18**, 1111.

93 S. S. Zhang and D. T. Tran, *J. Mater. Chem. A*, 2014, **2**, 7383.

94 K. Jeddi, K. Sarikhani, N. T. Qazvini and P. Chen, *J. Power Sources*, 2014, **245**, 656.

95 H. W. Chen, W. L. Dong, J. Ge, C. H. Wang, X. D. Wu, W. Lu and L. W. Chen, *Sci. Rep.*, 2013, **3**.

96 A. Konarov, D. Gosselink, T. N. L. Doan, Y. G. Zhang, Y. Zhao and P. Chen, *J. Power Sources*, 2014, **259**, 183.

97 S. S. Zhang, *Energies*, 2014, **7**, 4588.

98 Y. Z. Zhang, S. Liu, G. C. Li, G. R. Li and X. P. Gao, *J. Mater. Chem. A*, 2014, **2**, 4652.

99 L. L. Qiu, S. C. Zhang, L. Zhang, M. M. Sun and W. K. Wang, *Electrochim. Acta*, 2010, **55**, 4632.

100 L. C. Yin, J. L. Wang, F. J. Lin, J. Yang and Y. Nuli, *Energy Environ. Sci.*, 2012, **5**, 6966.

101 D. Aurbach, *J. Power Sources*, 2000, **89**, 206.

102 Y. Yang, G. Y. Zheng, S. Misra, J. Nelson, M. F. Toney and Y. Gui, *J. Am. Chem. Soc.*, 2012, **134**, 15387.

103 Z. C. Yang, J. C. Guo, S. K. Das, Y. C. Yu, Z. H. Zhou, H. D. Abruna and L. A. Archer, *J. Mater. Chem. A*, 2013, **1**, 1433.

104 S. Jeong, D. Bresser, D. Buchholz, M. Winter and S. Passerini, *J. Power Sources*, 2013, **235**, 220.

105 Y. Yang, M. T. McDowell, A. Jackson, J. J. Cha, S. S. Hong and Y. Cui, *Nano Lett.*, 2010, **10**, 1486.

106 J. Hassoun, Y. K. Sun and B. Scrosati, *J. Power Sources*, 2011, **196**, 343.

107 Y. Z. Fu, Y. S. Su and A. Manthiram, *Adv. Energy Mater.*, 2014, **4**.

108 K. P. Cai, M. K. Song, E. J. Cairns and Y. G. Zhang, *Nano Lett.*, 2012, **12**, 6474.

109 C. Y. Nan, Z. Lin, H. G. Liao, M. K. Song, Y. D. Li and E. J. Cairns, *J. Am. Chem. Soc.*, 2014, **136**, 4659.

110 Z. Lin, C. Nan, Y. Ye, J. Guo, J. Zhu and E. J. Cairns, *Nano Energy*, 2014, **9**, 408.

111 R. Elazari, G. Salitra, Y. Talyosef, J. Grinblat, C. Scordilis-Kelley, A. Xiao, J. Affinito and D. Aurbach, *J. Electrochem. Soc.*, 2010, **157**, A1131.

112 Q. Pang, D. Kundu, M. Cuisinier and L. F. Nazar, *Nat. Commun.*, 2014, **5**.

113 S. Z. Xiong, X. Kai, X. B. Hong and Y. Diao, *Ionics*, 2012, **18**, 249.

114 Z. Lin, Z. C. Liu, W. J. Fu, N. J. Dudney and C. D. Liang, *Adv. Funct. Mater.*, 2013, **23**, 1064.

115 S. S. Zhang, *J. Electrochem. Soc.*, 2012, **159**, A920.

116 X. Liang, Z. Y. Wen, Y. Liu, M. F. Wu, J. Jin, H. Zhang and X. W. Wu, *J. Power Sources*, 2011, **196**, 9839.

117 D. Aurbach, E. Pollak, R. Elazari, G. Salitra, C. S. Kelley and J. Affinito, *J. Electrochem. Soc.*, 2009, **156**, A694.

118 C. Huang, J. Xiao, Y. Y. Shao, J. M. Zheng, W. D. Bennett, D. P. Lu, S. V. Laxmikant, M. Engelhard, L. W. Ji, J. Zhang, X. L. Li, G. L. Graff and J. Liu, *Nat. Commun.*, 2014, **5**.

119 E. Peled, Y. Sternberg, A. Gorenshtein and Y. Lavi, *J. Electrochem. Soc.*, 1989, **136**, 1621.

120 D. R. Chang, S. H. Lee, S. W. Kim and H. T. Kim, *J. Power Sources*, 2002, **112**, 452.

121 J. W. Choi, J. K. Kim, G. Cheruvally, J. H. Ahn, H. J. Ahn and K. W. Kim, *Electrochim. Acta*, 2007, **52**, 2075.

122 H. S. Ryu, H. J. Ahn, K. W. Kim, J. H. Ahn, K. K. Cho, T. H. Nam, J. U. Kim and G. B. Cho, *J. Power Sources*, 2006, **163**, 201.

123 J. H. Shin and E. J. Cairns, *J. Power Sources*, 2008, **177**, 537.

124 H. Yamin, A. Gorenshtein, J. Penciner, Y. Sternberg and E. Peled, *J. Electrochem. Soc.*, 1988, **135**, 1045.

125 L. X. Yuan, J. K. Feng, X. P. Ai, Y. L. Cao, S. L. Chen and H. X. Yang, *Electrochem. Commun.*, 2006, **8**, 610.

126 J. W. Park, K. Ueno, N. Tachikawa, K. Dokko and M. Watanabe, *J. Phys. Chem. C*, 2013, **117**, 20531.

127 K. Ueno, J. W. Park, A. Yamazaki, T. Mandai, N. Tachikawa, K. Dokko and M. Watanabe, *J. Phys. Chem. C*, 2013, **117**, 20509.

128 J. Scheers, S. Fantini and P. Johansson, *J. Power Sources*, 2014, **255**, 204.

129 Y. Zhao, Y. Zhang, D. Gosselink, T. N. L. Doan, M. Sadhu, H.-J. Cheang and P. Chen, *Membranes*, 2012, **2**.

130 L. M. Suo, Y. S. Hu, H. Li, M. Armand and L. Q. Chen, *Nat. Commun.*, 2013, **4**.

131 W. Weng, V. G. Pol and K. Amine, *Adv. Mater.*, 2013, **25**, 1608.

132 M.-K. Song, Y. Zhang and E. J. Cairns, *Nano Lett.*, 2013, **13**, 5891.

133 S. F. Lux, F. Schappacher, A. Balducci, S. Passerini and M. Winter, *J. Electrochem. Soc.*, 2010, **157**, A320.

134 J. Sun, Y. Q. Huang, W. K. Wang, Z. B. Yu, A. B. Wang and K. G. Yuan, *Electrochim. Acta*, 2008, **53**, 7084.

135 Y. Wang, Y. Q. Huang, W. K. Wang, C. J. Huang, Z. B. Yu, H. Zhang, J. Sun, A. B. Wang and K. G. Yuan, *Electrochim. Acta*, 2009, **54**, 4062.

136 S. Y. Jiang, M. Y. Gao, Y. Q. Huang, W. K. Wang, H. Zhang, Z. B. Yu, A. B. Wang, K. G. Yuan and X. N. Chen, *J. Adhes. Sci. Technol.*, 2013, **27**, 1006.

137 M. M. Rao, X. Y. Song, H. G. Liao and E. J. Cairns, *Electrochim. Acta*, 2012, **65**, 228.

138 I. Kovalenko, B. Zdyrko, A. Magasinski, B. Hertzberg, Z. Milicev, R. Burtovyy, I. Luzinov and G. Yushin, *Science*, 2011, **334**, 75.

139 W. Z. Bao, Z. A. Zhang, Y. Q. Gan, X. W. Wang and J. Lia, *J. Energy Chem.*, 2013, **22**, 790.

140 C. X. Zu, Y. S. Su, Y. Z. Fu and A. Manthiram, *Phys. Chem. Chem. Phys.*, 2013, **15**, 2291.

141 Y. S. Su and A. Manthiram, *Chem. Commun.*, 2012, **48**, 8817.

142 Y. S. Su and A. Manthiram, *Nat. Commun.*, 2012, **3**.

143 K. Zhang, F. R. Qin, J. Fang, Q. Li, M. Jia, Y. Q. Lai, Z. A. Zhang and J. Li, *J. Solid State Electrochem.*, 2014, **18**, 1025.

144 X. F. Wang, Z. X. Wang and L. Q. Chen, *J. Power Sources*, 2013, **242**, 65.

145 J. Q. Huang, Q. Zhang, H. J. Peng, X. Y. Liu, W. Z. Qian and F. Wei, *Energy Environ. Sci.*, 2014, **7**, 347.

146 A. Vizintin, M. U. M. Patel, B. Genorio and R. Dominko, 2014, **1**, 1040.

147 S. S. Zhang, *J. Power Sources*, 2013, **231**, 153.

148 C. Barchasz, F. Molton, C. Duboc, J. C. Lepretre, S. Patoux and F. Alloin, *Anal. Chem.*, 2012, **84**,

3973.

149 Y. Diao, K. Xie, S. Z. Xiong and X. B. Hong, *J. Electrochem. Soc.*, 2012, **159**, A1816.

150 S. E. Cheon, S. S. Choi, J. S. Han, Y. S. Choi, B. H. Jung and H. S. Lim, *J. Electrochem. Soc.*, 2004, **151**, A2067.

151 T. A. Pascal, K. H. Wujcik, J. Velasco-Velez, C. H. Wu, A. A. Teran, M. Kapilashrami, J. Cabana, J. H. Guo, M. Salmeron, N. Balsara and D. Prendergast, *J. Phys. Chem. Lett.*, 2014, **5**, 1547.

152 N. A. Canas, S. Wolf, N. Wagner and K. A. Friedrich, *J. Power Sources*, 2013, **226**, 313.

153 J. Nelson, S. Misra, Y. Yang, A. Jackson, Y. J. Liu, H. L. Wang, H. J. Dai, J. C. Andrews, Y. Cui and M. F. Toney, *J. Am. Chem. Soc.*, 2012, **134**, 6337.

154 M. Agostini, D. J. Lee, B. Scrosati, Y. K. Sun and J. Hassoun, *J. Power Sources*, 2014, **265**, 14.

155 N. A. Canas, D. N. Fronczek, N. Wagner, A. Latz and K. A. Friedrich, *J. Phys. Chem. C*, 2014, **118**, 12106.

156 M. U. M. Patel, R. Demir-Cakan, M. Morcrette, J. M. Tarascon, M. Gaberscek and R. Dominko, *ChemSusChem*, 2013, **6**, 1177.

157 M. U. M. Patel and R. Dominko, *ChemSusChem*, 2014, **7**, 2167.

158 Q. Zhang, X. B. Cheng, J. Q. Huang, H. J. Peng and F. Wei, *New Carbon Mater.*, 2014, **29**, 241.

159 R. D. Rauh, K. M. Abraham, G. F. Pearson, J. K. Surprenant and S. B. Brummer, *J. Electrochem. Soc.*, 1979, **126**, 523.

160 Y. Yang, G. Zheng and Y. Cui, *Energy Environ. Sci.*, 2013, **6**, 1552.

161 C. Zu and A. Manthiram, *Adv. Energy Mater.*, 2014.

162 R. Demir-Cakan, M. Morcrette, Gangulibabu, A. Gueguen, R. Dedryvere and J.-M. Tarascon, *Energy Environ. Sci.*, 2013, **6**, 176.

163 F. Y. Fan, W. H. Woodford, Z. Li, N. Baram, K. C. Smith, A. Helal, G. H. McKinley, W. C. Carter and Y.-M. Chiang, 2014, **14**, 2210.

164 R. C. Agrawal and G. P. Pandey, *J. Phys. D-Appl. Phys.*, 2008, **41**.

165 E. Quartarone and P. Mustarelli, *Chem. Soc. Rev.*, 2011, **40**, 2525.

166 S. Z. Xiong, K. Xie, Y. Diao and X. B. Hong, *J. Power Sources*, 2014, **246**, 840.

167 H. Nagata and Y. Chikusa, *J. Power Sources*, 2014, **263**, 141.

168 S. Kinoshita, K. Okuda, N. Machida, M. Naito and T. Sigematsu, *Solid State Ionics*, 2014, **256**, 97.

169 M. Agostini, Y. Aihara, T. Yamada, B. Scrosati and J. Hassoun, *Solid State Ionics*, 2013, **244**, 48.

170 N. Kamaya, K. Homma, Y. Yamakawa, M. Hirayama, R. Kanno, M. Yonemura, T. Kamiyama, Y. Kato, S. Hama, K. Kawamoto and A. Mitsui, *Nat. Mater.*, 2011, **10**, 682.

171 T. Kobayashi, Y. Imade, D. Shishihara, K. Homma, M. Nagao, R. Watanabe, T. Yokoi, A. Yamada, R. Kanno and T. Tatsumi, *J. Power Sources*, 2008, **182**, 621.

172 J. E. Trevey, Y. S. Jung and S. H. Lee, *Electrochim. Acta*, 2011, **56**, 4243.

173 Z. Lin, Z. C. Liu, N. J. Dudney and C. D. Liang, *Acs Nano*, 2013, **7**, 2829.

174 R. Bouchet, S. Maria, R. Meziane, A. Aboulaich, L. Lienafa, J. P. Bonnet, T. N. T. Phan, D. Bertin, D. Gigmes, D. Devaux, R. Denoyel and M. Armand, *Nat. Mater.*, 2013, **12**, 452.

175 K. Jeddi, M. Ghaznavi and P. Chen, *J. Mater. Chem. A*, 2013, **1**, 2769.

176 D. Marmorstein, T. H. Yu, K. A. Striebel, F. R. McLarnon, J. Hou and E. J. Cairns, *J. Power Sources*, 2000, **89**, 219.

177 M. Nagao, Y. Imade, H. Narisawa, T. Kobayashi, R. Watanabe, T. Yokoi, T. Tatsumi and R. Kanno, *J. Power Sources*, 2013, **222**, 237.

178 K. Youngsik, N. Arumugam and J. B. Goodenough, *Chem. Mater.*, 2008, **20**, 470.
179 M. Nagao, A. Hayashi and M. Tatsumisago, *Electrochim Acta*, 2011, **56**, 6055.
180 J. Hassoun and B. Scrosati, *Adv. Mater.*, 2010, **22**, 5198.
181 X. A. Liang, Z. Y. Wen, Y. Liu, H. Zhang, L. Z. Huang and J. Jin, *J. Power Sources*, 2011, **196**, 3655.
182 Z. C. Liu, W. J. Fu, E. A. Payzant, X. Yu, Z. L. Wu, N. J. Dudney, J. Kiggans, K. L. Hong, A. J. Rondinone and C. D. Liang, *J. Am. Chem. Soc.*, 2013, **135**, 975.
183 Z. Lin, Z. Liu, W. Fu, N. J. Dudney and C. Liang, *Angew. Chem. Int. Ed.*, 2013, **52**, 7460.
184 A. Hayashi, T. Ohtomo, F. Mizuno, K. Tadanaga and M. Tatsumisago, *Electrochem. Commun.*, 2003, **5**, 701.
185 T. Takeuchi, H. Kageyama, K. Nakanishi, M. Tabuchi, H. Sakaebe, T. Ohta, H. Senoh, T. Sakai and K. Tatsumi, *J. Electrochem. Soc.*, 2010, **157**, A1196.

Biography & Photo

Zhan Lin received his Ph.D. in Fiber and Polymer Science at the North Carolina State University in 2010. After that, he worked as Postdoctoral Research Associate at Oak Ridge National Laboratory, and Postdoctoral Fellow at University of California-Berkeley/Lawrence Berkeley National Laboratory from 2011 to 2013. In 2014, he returned China under the "Thousand Youth Talents Program". He is currently Professor in the Department of Chemical & Biological Engineering at Zhejiang University. His research interests focus on nanostructured materials for Electrochemical Energy Storage and Conversion, including lithium-sulfur batteries, lithium-ion batteries, fuel cells, and solar cells.

Chengdu Liang received his PhD in Materials Chemistry and Analytical Chemistry at the University of Tennessee Knoxville in 2005. After a short period of postdoctoral research at the Chemical Science Division of Oak Ridge National Laboratory (ORNL), he started his career as a staff scientist at the Center for Nanophase Materials Sciences of ORNL in 2006. His research focuses on the synthesis of advanced materials for energy applications including lithium-ion batteries, lithium-sulfur batteries, solid electrolytes, sodium batteries, fuel cells, and heterogeneous catalysis.

Table of contents entry

Graphic

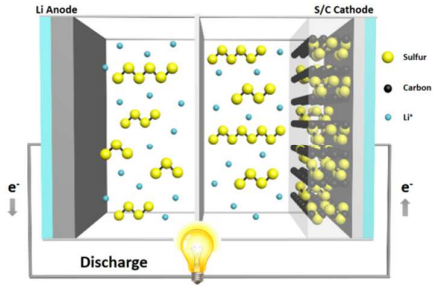

Text: This review article gives insights on the current status and future perspectives of the lithium-sulfur battery technology.